Landsat and Sentinel-derived glacial lake dataset in the China-Pakistan Economic Corridor from 1990 to 2020

Muchu Lesi[1], Yong Nie[1, *], Dan H. Shugar[2], Jida Wang[3], Qian Deng[1, 4], Huayong Chen[1], Jianrong Fan[1]

[1]Institute of Mountain Hazards and Environment, Chinese Academy of Sciences, Chengdu, China

[2]Water, Sediment, Hazards, and Earth-surface Dynamics (waterSHED) Lab, Department of Geoscience, University of Calgary, Alberta, T2N 1N4, Canada

[3]Department of Geography and Geospatial Sciences, Kansas State University, Manhattan, Kansas 66506, USA

[4]University of Chinese Academy of Sciences, Beijing 100190, China

[*]Corresponding author, nieyong@imde.ac.cn

Abstract. The China-Pakistan Economic Corridor (CPEC) is one of the flagship projects of the One Belt One Road Initiative, which faces threats from water shortage and mountain disasters in the high-elevation region, such as glacial lake outburst floods (GLOFs). An up-to-date high-quality glacial lake dataset with parameters such as lake area, volume, and type, which is fundamental to water resource and flood risk assessments, and predicting glacier-lake evolutions, is still largely absent for the entire CPEC. This study describes a glacial lake dataset for the CPEC using a threshold-based mapping method associated with rigorous visual inspection workflows. This dataset includes (1) multi-temporal inventories for 1990, 2000, and 2020 produced from 30 m resolution Landsat images, and (2) a glacial lake inventory for the year 2020 at 10 m resolution produced from Sentinel-2 images. The results show that, in 2020, 2234 lakes were derived from the Landsat images, covering a total area of 86.31 ± 14.98 km^2 with a minimum mapping unit of 5 pixels (4500 m^2), whereas 7560 glacial lakes were derived from the Sentinel-2 images with a total area of 103.70 ± 8.45 km^2 with a minimum mapping unit of 5 pixels (500 m^2). The discrepancy shows that Sentinel-2 ~~is able to~~can detect a significant quantity of smaller lakes than Landsat due to its finer spatial resolution. Glacial lake data in 2020 was validated by Google Earth-derived lake boundaries with a median (±standard deviation) difference of 7.66 ± 4.96 % for Landsat-derived product and 4.46 ± 4.62 % for Sentinel-derived product. The total number and area of glacial lakes from consistent 30 m resolution Landsat images remain relatively stable despite a slight increase from 1990 to 2020. A range of critical attributes ~~have~~ has been generated in the dataset, including lake types and mapping uncertainty estimated by an improved Hanshaw's equation. This comprehensive glacial lake dataset has the potential to be widely applied in studies on water resource assessment, glacial lake-related hazards, and glacier-lake interactions, and is freely available at https://doi.org/10.12380/Glaci.msdc.000001 (Lesi et al., 2022).

1 Introduction

Glaciers in High-mountain Asia (HMA) play a crucial role in regulating climate, supporting ecosystems, modulating the release of freshwater into rivers, and sustaining municipal water supplies (Wang et al., 2019; Viviroli et al., 2020), agricultural irrigation, and hydropower generation (Pritchard, 2019; Nie et al., 2021). Most HMA glaciers are losing mass in the context of climate change (Brun et al., 2017; Maurer et al., 2019; Shean et al., 2020; Bhattacharya et al., 2021), therefore, unsustainable glacier melt and the passing of peak water are reducing the hydrological role of glaciers (Huss and Hock, 2018) and impacting downstream ecosystem services, agriculture, hydropower and other socioeconomic values (Carrivick and Tweed, 2016; Nie et al., 2021). The present and future glacier changes not only impact the water supply for the downstream area but also alter the frequency and intensity of glacier-related hazards, such as glacier lake outburst floods (GLOFs) (Nie et al., 2018; Rounce et al., 2020; Zheng et al., 2021), and rock and ice avalanches (Shugar et al., 2021). Global glacial lake number and total area both increased between 1990 and 2018 in response to glacier retreat and climate change (Shugar et al., 2020), affecting the allocation of freshwater resources. The Indus is globally the most important and vulnerable water tower unit where glaciers, lakes, and reservoir storage contribute about two-thirds of the water supply (Immerzeel et al., 2020). Ice-marginal lakes store ~1% of total ice discharge in

63 Greenland and accelerate lake-terminating ice velocity by ~25% (Carrivick et al., 2022). An
64 increasing frequency and risk of GLOFs (Nie et al., 2021; Zheng et al., 2021) is threatening
65 the Asian population and infrastructures in the mountain ranges, such as the China-Pakistan
66 Economic Corridor (CPEC), as a flagship component of One Belt One Road Initiative
67 (Battamo et al., 2021; Li et al., 2021). The northern section of the CPEC passes through
68 Pamir, Karakoram, Hindu Kush, and Himalaya mountains where droughts and glacier-related
69 hazards are frequent and severe (Hewitt, 2014; Bhambri et al., 2019; Pritchard, 2019),
70 threatening local people, the existing, under-construction and planned infrastructures, such as
71 highways, hydropower plants, and railways. Understanding the risk posed by water shortage
72 and glacier-related hazards is a critical step toward sustainable development for the CPEC.
73   Glacial lake inventories with a range of attributes benefit water resource assessment and
74 disaster risk assessment related to glacial lakes (Wang et al., 2020; Carrivick et al., 2022),
75 and contribute to predicting glacier-lake evolution and cryosphere-hydrosphere interactions
76 under climate change (Nie et al., 2017; Brun et al., 2019; Maurer et al., 2019; Carrivick et al.,
77 2020; Liu et al., 2020). Remote sensing is the most viable way to map glacial lakes and detect
78 their spatio-temporal changes in the high-elevation zones where in situ accessibility is
79 extremely low (Huggel et al., 2002; Quincey et al., 2007). Studies in glacial lake inventories
80 using satellite observations have been heavily conducted at regional scales recently, such as
81 in the Tibetan Plateau (Zhang et al., 2015), the Himalaya (Gardelle et al., 2011; Nie et al.,
82 2017), the HMA (Wang et al., 2020; Chen et al., 2021), the Tien Shan (Wang et al., 2013),
83 the Alaska (Rick et al., 2022), the Greenland (How et al., 2021) and the northern Pakistan
84 (Ashraf et al., 2017). However, the latest glacial lake mapping in 2020 is still absent along the
85 CPEC. Among existing studies, Landsat archival images are the most widely used due to their
86 multi-decadal record of earth surface observations, reasonably high spatial resolution (30 m),
87 and publicly available distribution (Roy et al., 2014). Freely available Sentinel-2 satellite
88 images show a better potential than Landsat in glacial lake mapping and inventories due to
89 their higher spatial resolution (10 m) and a global coverage, but have only been available
90 since late 2015 (Williamson et al., 2018; Paul et al., 2020). Glacial lake inventories using
91 Sentinel-2 images are relatively scarce at regional scales, and studies of the latest glacial lake
92 mapping as well as comparisons of glacial lake datasets derived from Sentinel-2 and Landsat
93 observations are still lacking.
94   Discrepancies between various glacial lake inventories (Zhang et al., 2015; Shugar et al.,
95 2020; Wang et al., 2020; Chen et al., 2021; How et al., 2021) result from differences in
96 mapping methods, minimum mapping units, the definition of glacial lakes, time periods, data
97 sources and other factors. For example, the manual vectorization method was widely adopted
98 at the earlier stage for its high accuracy. However, it is time-consuming associated with high
99 labor intensity, and is only practical at regional scales (Zhang et al., 2015; Wang et al., 2020).
100 Automated and semi-automated lake mapping methods, such as multi-spectral index
101 classification (Gardelle et al., 2011; Nie et al., 2017; Zhang et al., 2018; How et al., 2021),
102 have been developed to improve the efficiency of glacial lake inventories using optical
103 images, although manual modification is often unavoidable to assure the quality of lake data
104 impacted by cloud cover, mountain shadows, seasonal snow cover and frozen lake surfaces
105 (Sheng et al., 2016; Wang et al., 2017, 2018). Backscatter images from Synthetic Aperture
106 Radar (SAR) (Wangchuk and Bolch, 2020; How et al., 2021) were used to remove the impact

107 of cloud cover for lake mapping. Besides, other approaches such as hydrological sink
108 detection using DEM (How et al., 2021) and land surface temperature-based detection
109 method (Zhao et al., 2020) were also used for lake inventories. Different classification
110 methods impact the results of lake mapping and monitoring. So far, we are lacking a unified
111 standard for the classification system of glacial lakes (Yao et al., 2018). Existing
112 classification systems are generally used for their ~~individual~~ research purposes, mainly based
113 on the relative positions of glacial lakes and glaciers, the supply conditions of glaciers, and
114 the attributes of dams. In addition to different classification standards, the same type of
115 glacial lakes may also have different names given by different scholars. For example, ice-
116 marginal (Carrivick and Quincey, 2014; Carrivick et al., 2020), ice-contact (Carrivick and
117 Tweed, 2013), and proglacial (Nie et al., 2017) lakes all represent glacial lakes sharing the
118 boundary with glaciers. Glacier lakes in currently available datasets have been traditionally
119 categorized by their spatial relationship with upstream glaciers (Gardelle et al., 2011; Wang
120 et al., 2020; Chen et al., 2021), and classification attributes considering the formation
121 mechanism and the properties of dams are rare or incomplete in the CPEC (Yao et al., 2018;
122 Li et al., 2020). ~~Dam~~ Dam-type classification of glacial lakes provides a crucial attribute for
123 glacier-lake interactions and risk assessment (Emmer and Cuřín, 2021). Therefore, an up-to-
124 date glacial lake dataset with critical, quality-assured parameters (e.g. lake area, volume, and
125 type) is necessary.
126   This study aims to (1) present an up-to-date glacial lake dataset in the CPEC in 2020 using
127 both Landsat 8 and Sentinel-2 images to accurately document its detailed lake distribution;
128 (2) present two historical glacial lake datasets for the CPEC to show the extent in 1990 and
129 2000 using consistent 30-m Landsat images to reveal glacial lake changes at three time
130 periods (1990, 2000 and 2020); and (3) generate a range of critical attributes for glacial lake
131 inventories to benefit studies on water resource evaluation, risk assessment of GLOFs, glacier
132 –lake evolution modeling in the HMA.
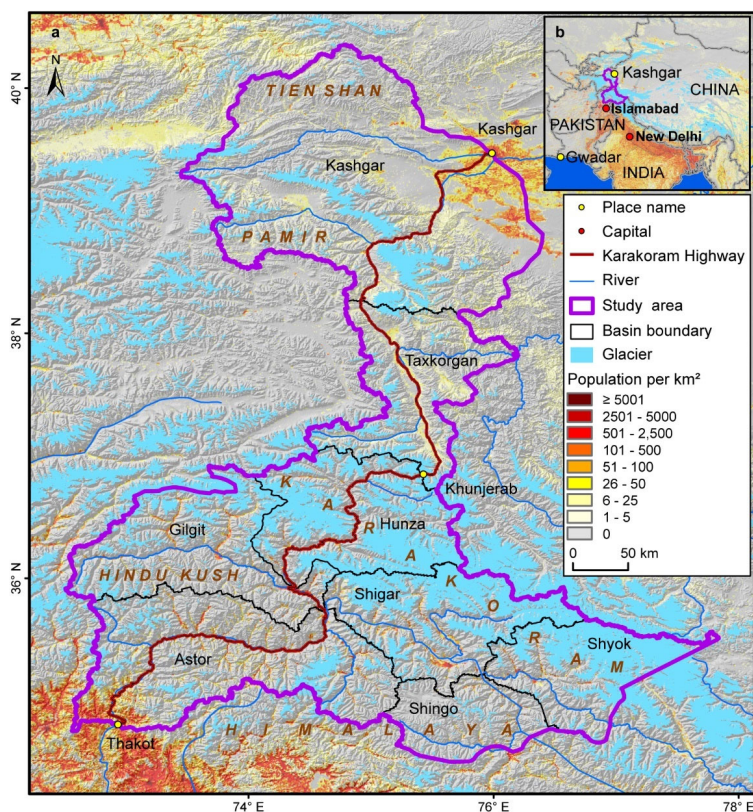
2 Study area

Figure 1. Location of the study area associated with the distribution of glaciers (RGI Consortium, 2017), mountains, basins, and population (Rose et al., 2021) (a), and its location within the CPCE (b).

The northern part of the CPEC is selected as the study area (Figure 1Figure 1). The CPCE, originating from Kashgar of the Xinjiang Uygur Autonomous region, China and extending to Gwadar Port, Pakistan (Ullah et al., 2019; Yao et al., 2020), is connecting China and Pakistan via the only Karakoram Highway. The study area covers all the drainage basins along Karakoram Highway starting from Kashgar and ending at Thakot, with a total area of ~125,000 km^2. The upper Indus basins beyond the Pakistani-administrated border are excluded in from this study due to the spatial coverage of the CPCE. The entire study area is divided into eight sub-basins, covering most of the Karakoram with the highest elevation up to 8611 m, western Himalaya and Tien Shan, eastern Hindu Kush, and the Pamir Mountains. The 9710 glaciers in the study area cover a total area of 17,447 km^2 and nearly 60% of glaciers are distributed in the Karakoram (5818 glaciers with a total area of 14,067.52 km^2) (RGI Consortium, 2017). Most glaciers in the western Himalaya and eastern Hindu Kush are losing mass in the context of

带格式的: 字体: 非加粗

climate change (Kääb et al., 2012; Yao et al., 2012; Brun et al., 2017; Shean et al., 2020; Hugonnet et al., 2021), whereas the glaciers in the eastern Karakoram and Pamir have shown unusually little changes, including unchanged, retreated, advanced and surged glaciers (Hewitt, 2005; Kääb et al., 2012; Bolch et al., 2017; Brun et al., 2017; Shean et al., 2020; Nie et al., 2021). The spatially heterogeneous distribution and changes of glaciers are primarily explained as a result of differences in the dominant precipitation-bearing atmospheric circulation patterns that include the winter westerlies the Indian summer monsoon, their changing trends, and their interactions with local extreme topography (Yao et al., 2012; Azam et al., 2021; Nie et al., 2021).

3 Data sources

Both Landsat and Sentinel-2 images have been employed to map glacial lakes between 1990 and 2020 in the CPEC (Figure 2Figure 2). A total number of 71 Landsat Thematic Mapper (TM), Thematic Mapper Plus (ETM+), and Landsat 8 Operational Land Imager (OLI) images with a consistent spatial resolution of 30 m were downloaded from the United States Geological Survey Global Visualization Viewer (GloVis, https://glovis.usgs.gov/) to be used to create glacial lake inventories in 1990, 2000 and 2020. High-quality Landsat-5 images around 2010 are insufficient to cover the entire study area, so we were unable to map lakes in 2010 due to Landsat-7's scan-line corrector errors and significant cloud covers. In addition, 39 Sentinel-2 images (23 scenes in 2020) were downloaded from Copernicus Open Access Hub (https://scihub.copernicus.eu/) to produce the 10-m resolution glacial lake inventory in 2020. All images used in this study have been orthorectified before download, but we still find that one Sentinel-2 image was not well matched with Landsat images, leading to the discrepancy between the two glacial lake datasets. We manually georeferenced the shifted image to minimize the difference between Sentinel- and Landsat Landsat-derived glacial lakes.

Cloud and snow coverss heavily affect the usability of optical satellite images (Wulder et al., 2019) and their availability in the entire study area, so we took advantage of the images acquired before and after each of the baseline years 1990, 2000 and 2020 to construct the glacial lake inventories. Only 4 images in 1990 (the largest covering the study area), 16 images in 2000, and 23 images in 2020 were used for matching baseline year. Spatially, high-quality images in given baseline years were preferentially chosen, or we selected one or more alternative images acquired in adjacent years to delineate glacial lakes by removing the effect of cloud and snow covers. To minimize the impact of intra-annual changes of on glacial lakes, most of the used images (82% for Sentinel-2 and 75% for Landsat) were acquired from August to October in the given baseline year with cloud coverage of <20% for each image. For some specific scenes where cloud cover exceeded the threshold of 20%, we selected more than one image to remedy the effect of cloud contamination (Nie et al., 2010, 2017; Jiang et al., 2018).

Other datasets used include the Randolph Glacier Inventory version 6.0 (Pfeffer et al., 2014; RGI Consortium, 2017) and the Glacier Area Mapping for Discharge from the Asian Mountains (GAMDAM) glacier inventory (Sakai, 2019). These two glacier datasets were used to determine glacial lake types, such as ice-contact, ice-dammed, and unconnected-glacier-fed lakes. The Shuttle Radar Topography Mission Digital Elevation Model (SRTM

带格式的: 字体: (中文) 宋体, 非加粗

193 DEM) at a 1-arc second (30 m) resolution (Jarvis et al., 2008) was employed to extract the
194 altitudinal characteristics of the glacial lakes. The absolute vertical accuracy of the SRTM
195 DEM is 16 m (90%) (Rabus et al., 2003; Farr et al., 2007). We also applied other published
196 glacial lake datasets for comparative analysis. They include the glacial lake inventories of
197 HMA in 1990 and 2018 downloaded from http://doi.org/10.12072/casnw.064.2019.db (Wang
198 et al., 2020), the Third Pole region in 1990, 2000, and 2010 publicly shared at
199 http://en.tpedatabase.cn/ (Zhang et al., 2015), the Tibet Plateau from 2008 to 2017 accessed at
200 https://doi.org/10.5281/zenodo.3700282 (Chen et al., 2021), and the entire world in 1990,
201 2000 and 2015 provided at https://nsidc.org/data /HMA_ GLI/versions/1 (Shugar et al.,
202 2020). In addition, field survey data collected between 2017 and 2018 were also used to assist
203 in lake mapping and glacial lake type classification.

204

205
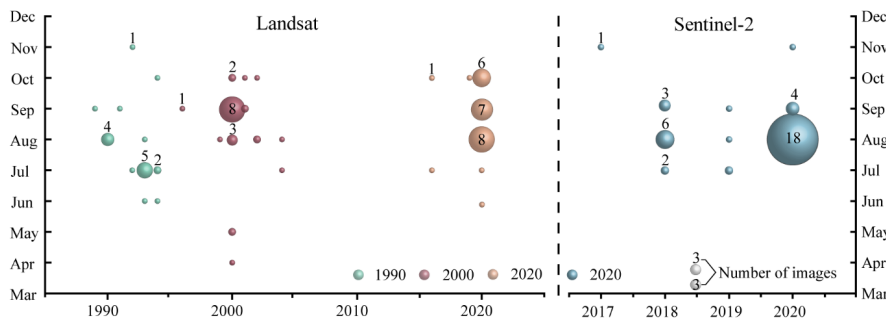
Figure 2. Acquisition of years and months of Landsat and Sentinel-2 images selected for glacial lake
inventories. The bubble size indicates the available high-quality image number.

4 Glacial lake inventory methods

4.1 Definition of glacial lakes

210 We consider a glacial lake as one that formed as a result of modern or ancient glaciation.
211 Contemporary glacial lakes are easily recognized using a combination of glacier inventories
212 and remote sensing images. Ancient glacial lakes can be identified from periglacial
213 geomorphological characteristics, including moraine remnants and U-shaped valleys that are
214 discernible from satellite observations (Post and Mayo, 1971; Westoby et al., 2014; Nie et al.,
215 2018; Martín et al., 2021). A 10-km buffering distance of RGI 6.0 glacier boundaries that has
216 been widely used in previous studies (Zhang et al., 2015; Wang et al., 2020), was created to
217 help mapping glacial lakes. A few glacial lakes in the study area (a total of 84 lakes for the
218 Sentinel-2 dataset and 55 lakes for the Landsat dataset in 2020) beyond the buffering zone,
219 located near buffering boundaries, were intentionally included due to clear evidence of
220 glaciation (Figure 3Figure 3). Landslide-dammed lakes (Chen et al., 2017) in the buffering
221 zone were excluded in from our inventories because of their irrelevance to glaciation. All
222 glacial lakes in the study area were mapped according to our definition. We were able to
223 implement this definition by carefully leveraging the spectral properties of glacial lakes and
224 the periglacial geomorphological features that are often evident in remote sensing images (see

225 more in sections 4.3 and 4.4).

226

227

228
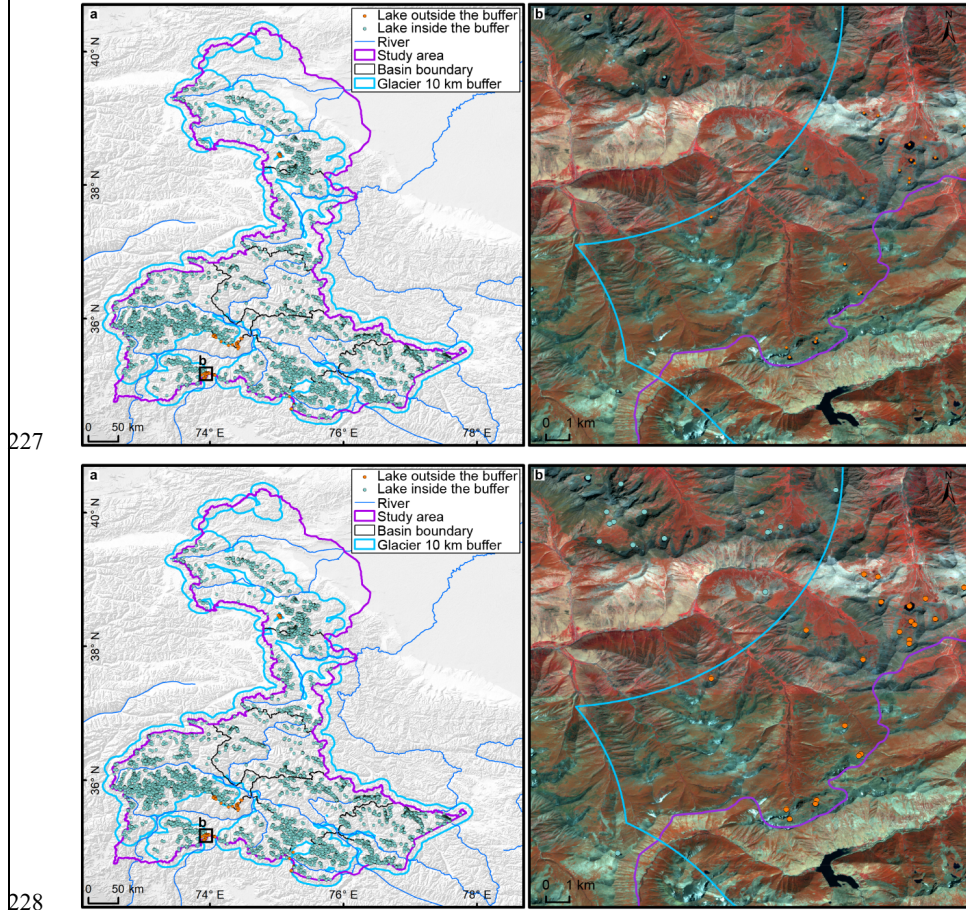
Figure 3. The 10-km buffer zone of RGI 6.0 glacier boundaries (a) and Sentinel-derived glacial lakes
230 located near buffering boundary within the study area (b).

231

232 4.2 Interactive lake mapping

233 A human-interactive and semi-automated lake mapping method (Wang et al., 2014; Nie et al.,
234 2017, 2020) was adopted to accurately extract glacial lake extents using Landsat and
235 Sentinel-2 images, based on the Normalized Difference Water Index (NDWI) (Mcfeeters,
236 1996). The NDWI uses the green and ~~near~~ near-infrared bands and is calculated by the
237 following equation:

238
$$NDWI = \frac{Band_{Green} - Band_{NIR}}{Band_{Green} + Band_{NIR}} \qquad \underline{\hspace{2cm}} \qquad (1)$$

239 where the green band and ~~near~~ near-infrared band were provided by both Landsat and
240 Sentinel multispectral images.

241   Specifically, the method calculated the NDWI histogram based on the pixels with each
242 user-defined and manually-drawn region of interest. The NDWI threshold that separates the
243 lake surface from the land was interactively determined by screening the NDWI histogram
244 against the lake region in the imagery (Wang et al., 2014; Nie et al., 2020). This way, the
245 determined NDWI threshold can be well-tuned to adapt to various spectral conditions of the
246 studied glacier lakes. The raster lake extents segmented by the thresholds were then
247 automatically converted to vector polygons. We first completed the glacial lake inventory in
248 2020 using this interactive mapping method, and the 2020 inventory was then used as a
249 reference to facilitate the lake mapping for other periods.

250   The minimum mapping unit (MMU) was set to 5 pixels for both Landsat (0.0045 km^2) and
251 Sentinel-2 images (0.0005 km^2) in this study. MMU determines the total number and area of
252 glacial lakes in the dataset, and varies in the previous studies, such as 3 pixels (Zhang et al.,
253 2015), 6 pixels (Wang et al., 2020), or 9 pixels (Chen et al., 2021) for a regional scale, or 55
254 pixels (Shugar et al., 2020) for a global scale. While a smaller threshold leads to a large
255 ~~quantity~~ number of lakes mapped, it also generates larger mapping noises or uncertainties.
256 Considering this signal-noise balance and our focus on identifying prominent glacier lake
257 dynamics in the study area, we opted to use 5 pixels as the MMU for both Landsat and
258 Sentinel-2 images.

259   Several procedures were taken to assure the quality assurance and quality control for lake
260 mapping, including 1) visual inspection and modification using the threshold-based mapping
261 method for each lake according to Landsat, Sentinel-2, and Google Earth high-resolution
262 images overlaying preliminarily lake boundary extraction at the given ~~time~~ period; 2) time
263 series check for Landsat-derived glacial lake datasets from 1990 and 2020, and cross-check
264 between Landsat and Sentinel-2-derived lake dataset in 2020 to reduce errors of omission and
265 commission; 3) topological validation of glacial lake mapping, such as repeated removal,
266 elimination of small sliver polygons; and 4) logical check for lake types between two
267 classification systems of glacial lakes. False lake extents resulting from cloud or snow cover,
268 lake ice, and topographic shadows (Nie et al., 2017, 2020) were modified using the previous
269 semi-automated mapping method based on alternative images acquired in adjacent years.
270 Those procedures were time-consuming, but helped to minimize the effect of cloud and snow
271 covers, and lake mapping errors, and to maximize the quality of the produced lake product
272 and the derived glacial lake changes.

273 4.3 Classification of glacial lakes

274 Two glacial lake classification systems (GLCS) have been established based on the
275 relationship of interaction between glacial lakes and glaciers as well as lake formation
276 mechanism and dam material properties. In the first GLCS (GLCS1), glacial lakes were
277 classified into four types based on their spatial relationship to upstream glaciers: supraglacial,
278 ice-contact, unconnected-glacier-fed lakes, and non-glacier-fed lakes according to Gardelle et
279 al. (2011) and Carrivick et al. (2013). Alternatively, combining the formation mechanism of
280 glacial lakes and the properties of natural dam features, glacial lakes were classified into five
281 categories (herein named GLCS2) modified from Yao's classification system (2018):
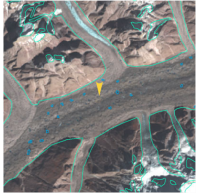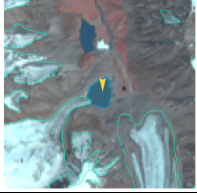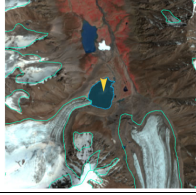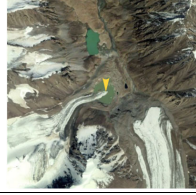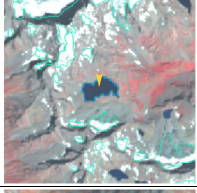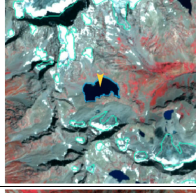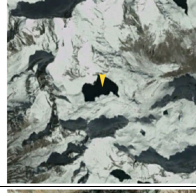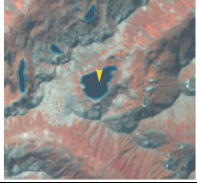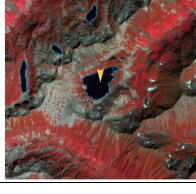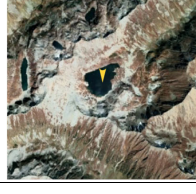
282 supraglacial, end-moraine-dammed, lateral-moraine-dammed, glacial-erosion lakes and ice-
283 dammed lakes. Subglacial lakes were excluded due to the mapping challenge from spectral
284 satellite images alone. Characterization and examples for each type are provided in Table
285 1Table 1 and Table 2Table 2. Individual glacial lakes were categorized into the specific types
286 for each GLCS according to available glacier inventory data, and geomorphological and
287 spectral characteristics interpreted from Landsat, Sentinel, and Google Earth images. The
288 synergy of these two GLCSs is beneficial to predicting glacier-lake evolutions and providing
289 fundamental data for water resource and glacial lake disaster risk assessment.
290

291
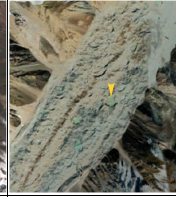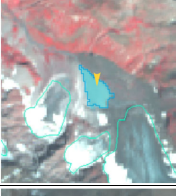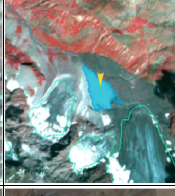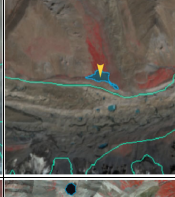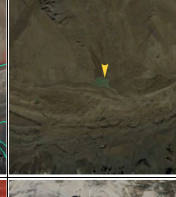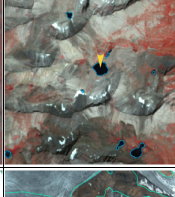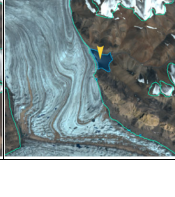
Table 1. ~~Classification~~ A classification system of glacial lake types (GLCS1) according to the relationship between glacial lakes and glaciers (© Google Earth 2019). Glacier outlines are from RGI 6.0 (RGI Consortium, 2017), and the yellow marker represents the target lake.

Lake types	Characteristics	Landsat	Sentinel-2	Google Earth
Supraglacial	Lakes formed on the surface of glaciers, generally dammed by ice and thin debris. Case location: 35°43'49.74" N 76°13'53.88" E			
Ice-contact	Lakes are dammed by moraine, ice, or bedrock, supplied by glacial meltwater, and shared boundary with glaciers. Case location: 39°09'32.40" N 73°43'12.00" E			
Unconnected-glacier-fed	Lakes are currently supplied by upstream glacial meltwater but disconnected ~~with~~ from glaciers. Case location: 35°47'60.00" N 72°55'15.60" E			
Non-glacier-fed	Lakes formed by glaciology, dammed by moraine or bed rock, and currently not supplied by glacial meltwater. Case location: 34°50'39.99" N 74°48'29.31" E			

295

Table 2. ~~Classification~~ A classification system of glacial lake types (GLCS2) according to the formation mechanism of glacial lakes and dam material properties (© Google Earth 2019). ~~Glacier~~ The glacier outlines from RGI 6.0 (RGI Consortium, 2017), and the yellow marker represents the target lake.

Lake types	Characteristics	Landsat	Sentinel-2	Google Earth
Supraglacial	Lakes formed on the surface of glaciers, generally dammed by ice and thin debris. Case location: 36°46'7.39" N 74°20'7.59" E			
End-moraine-dammed	Lakes formed behind moraines as a result of glacier retreat and downwasting. Case location: 35°42'50.40" N 73°09'57.60" E			
Lateral-moraine-dammed	Lakes formed behind lateral glacial moraine ridges and are dammed by debris, different from an ice-dammed glacial lake. Case location: 38°28'45.62" N 75°20'52.30" E			
Glacial-erosion	Lakes formed in depressions created by glacial over-deepening. Bedrock dam dominates, partially superimposed by top moraine in rugged terrain. Dams are unclear in the satellite images. Case location: 35°55'55.56" N 73°38'20.13" E			
Ice-dammed	Lakes formed behind glaciers, dammed by glacier ices (partially covered by debris on the top). Case location: 35°28'31.32" N 77°30'46.81" E			

4.4 Attributes of glacial lake data

A total of 18 attribute fields were input into our glacial lake datasets (Table 3~~Table 3~~). They include lake location (longitude and latitude), lake elevation (centroid elevation), orbital number of the image source, image acquisition date, lake area, lake perimeter, lake types of the two GLCSs, mapping uncertainty, lake water volume and the country, sub-basin, and mountain range associated with the lake. Amongst the attributes, lake location was calculated based on

带格式的: 字体: 非加粗

306 the centroid of each glacial lake polygon associated with the DEM, N represents northing and
307 E represents easting. ~~Orbital~~ The orbital number of the image source was filled with the
308 corresponding satellite image, with the codes expressed as "PxxxRxxx" or "Txxxxx", where P
309 and R indicate the path and row for Landsat image and T represents the tile of Sentinel-2 image
310 associated with 5 digit code of military grid reference system. SceneID indicated identifying
311 information of image source for Landsat or Sentinel-2, ~~consisted~~ consisting of the orbital
312 number, sensor ID, and acquisition date (YYYYMMDD) for Landsat image, or the orbital
313 number and acquisition date (YYYYMMDD) for Sentinel-2 image. Area and perimeter were
314 automatically calculated based on glacial lake extents. Lake water volume was estimated by an
315 area-volume empirical equation (Cook and Quincey, 2015). Lake types were attributed using
316 the characterization and interpretation marks described in Section 4.3. Mapping uncertainty
317 was estimated using our modified equation which will be introduced in section 4.5 and the
318 appendix tutorial. Located country, sub-basin, and the mountain range of each glacial lake ~~was~~
319 were identified by overlapping the geographic boundaries of countries, basins, and mountain
320 ranges.
321
322 **Table 3.** Attributes of glacial lake dataset.

Field Name	Type	Description	Note
FID or OBJECTID	Object ID	Unique code of glacial lake	Number
Shape	Geometry	Feature type of glacial lake	Polygon
Latitude	String	Latitude of the centroid of glacial lake polygon	Degree minute second
Longitude	String	Longitude of the centroid of glacial lake polygon	Degree minute second
Elevation	Double	Elevation of the centroid of glacial lake polygon	Unit: meter above sea level
SceneID	String	Scene ID of image source for Landsat or Sentinel-2	PxxxRxxx_xxxDYYYYMMDD or Txxxxx_YYYYMMDD
ACQDATE	String	~~Acquisition~~ The acquisition date of the source image	YYYYMMDD
GLCS1	String	The first classification system of glacial lakes based on the relationship of interaction between glacial lakes and glaciers	Supraglacial, Ice-contact, Unconnected-glacier-fed, None-glacier-fed
GLCS2	String	The second classification system of glacial lakes is based on lake formation mechanism and dam material properties	Supraglacial, End-moraine-dammed, Lateral-moraine-dammed, Glacial-erosion and Ice-dammed

Field Name	Type	Description	Note
Basin	String	Basin name where the glacial lake locates in	
Mountain	String	Mountain name where the glacial lake locates in	
Country	String	Country name where the glacial lake locates in	
Perimeter	Double	~~Perimeter~~ The perimeter of the glacial lake boundary	Unit: meter
Area	Double	Area of glacial lake coverage	Unit: square meter
AreaUncer	Double	Area uncertainty of glacial lake mapping estimated based on modified Hanshaw's equation (2014)	Unit: square meter
Operator	String	~~Operator~~ The operator of the glacial lake dataset	Muchu, Lesi
Examiner	String	Examiner of glacial lake dataset	Yong, Nie
Volume	Double	~~Water~~ The water volume of a glacial lake estimated by an area-volume empirical equation	Unit: cubic meter

323

324 4.5 Error and uncertainty assessment

325 4.5.1 Improved uncertainty estimating method

326 We modified Hanshaw's (2014) equation that had been used to calculate lake-area mapping
327 uncertainty. Lake perimeter and displacement error are widely used to estimate the
328 uncertainty of glacier and lake mapping from satellite observation (Carrivick and Quincey,
329 2014; Hanshaw and Bookhagen, 2014; Wang et al., 2020). Hanshaw and Bookhagen (2014)
330 proposed an equation to calculate the error of area measurement by the number of edge pixels
331 of the lake boundary multiplied by half of a single pixel area. The number of edge pixels is
332 simply calculated by the perimeter divided by the grid size. The equation is expressed ~~as~~
333 below:

334
$$Error(1\sigma) = \frac{P}{G} \times 0.6872 \times \frac{G^2}{2} \qquad \underline{} \qquad (2)$$

335
$$D = \frac{Error(1\sigma)}{A} \times 100\% \qquad \underline{} \qquad (3)$$

Where G is the cell size of the remote sensing imagery (10 m for Sentinel-2 image and 30 m for Landsat image). P is the perimeter of individual glacial lake (m), and the coefficient of 0.6872 (1σ), which means nearly 69% of the edge pixels are subject to errors (Hanshaw and Bookhagen, 2014), was chosen assuming that area measurement errors follow a Gaussian distribution. Relative error (D) was calculated by equation 3, in which A is the area of an individual glacial lake.

In the original equation 2, the number of edge pixels varies by the shape of the lake and is indicated by $\frac{P}{G}$. However, the pixels in the corner are ~~double~~ double-counted (Figure 4~~Figure 4~~). The total number of repeatedly calculated edge pixels equals the number of inner nodes. Therefore, we adjusted the calculation of the actual number of edge pixels as the maximum of edge pixels ($\frac{P}{G}$) subtracting the number of inner nodes. Accordingly, the equation of uncertainty estimation for lake mapping is modified as below:

$$Error(1\sigma) = (\frac{P}{G} - N_{Inner}) \times 0.6872 \times \frac{G^2}{2} \qquad (4)$$

Where N_{Inner} is the number of inner nodes (inflection points) of each lake. The modified equation is also suitable for lakes with islands (as illustrated in Figure 4~~Figure 4~~b).

For polygons without islands (Figure 4~~Figure 4~~a), use the following equation:

$$N_{Inner} = (\frac{N_{Total} - 4 - 1}{2}) \qquad (5)$$

N_{Total} is the total number of nodes, including both the outer and inner. N_{Total} is calculated by the "Field Calculator" in ArcGIS, in some cases, it is necessary to remove the redundant nodes before calculating the total number of nodes (See the Appendix for more details). An inner node is a polygon vertex where the interior angle surrounding it is greater than 180 degrees. An outer node is the opposite of the inner node, where the interior angle is less than 180 degrees. We found that the outer nodes are usually four more than the inner nodes in our glacial lake dataset. The total nodes in ArcGIS contain one overlapping node to close the polygon, meaning the endpoint is also the start point. This extra count was deleted ~~in~~ from the calculation (equation 5).

For polygons with island (Figure 4~~Figure 4~~b) use the following equation:

$$N_{Inner} = (\frac{N_{Total} - (N_{Island} + 1) \times 5}{2}) \qquad (6)$$

N_{Island} is the number of islands within each polygon. A calculation method of N_{Island} is given in the Appendix.

Lake Non-water pixel • Inner node
Edge pixel Double counted pixel Lake boundary
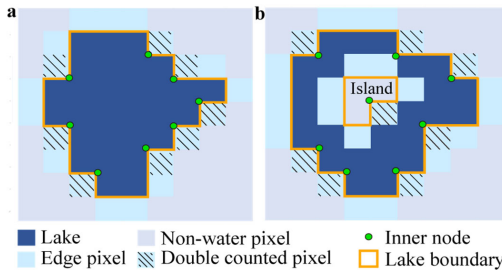
Figure 4. Sketch of estimating the actual edge pixels for uncertainty calculation of individual glacial lakes (with (a) and without islands (b)).

4.5.2 Validation of glacial lake mapping

A total of 89 glacial lakes were selected by stratified random sampling and manually digitized based on the Google Earth images in circa 2020 with a spatial resolution of ～2 m acquired from WorldView, GeoEye, Pleiades, etc. satellites to further validate the absolute error of our glacial lake products in 2020 due to lacking of field measurements for glacial lakes in the study area. During the sampling, we set a minimum lake area to be 4500 m^2 and a relative difference between Landsat- and Sentinel-derived lake areas of less than 18% (nearly equaling to the average relative error of ±17.36% for Landsat lake mapping) in order to minimize the effect of lake changes from multi-temporal satellite observations in circa 2020. The 89 sample lakes range from 0.005 km^2 to 0.802 km^2 with a median (standard deviation) size of 0.047±0.134 km^2 and a total area of 8.033 km^2 for Landsat-derived dataset, and range from 0.005 km^2 to 0.849 km^2 with a median (standard deviation) size of 0.045±0.144 km^2 and a total area of 8.447 km^2 for Sentinel-derived dataset.

5 Results

5.1 Glacier lake distribution and changes observed from Landsat

We mapped 2,234 glacial lakes for 2020 across the studied CPEC from Landsat-8 images, with a total area of 86.31±14.98 km^2 (Figure 5Figure 5a and b). Unconnected-glacier-fed lakes are dominant in the first classification system, followed by non-glacier-fed lakes (Figure 6Figure 6) whereas glacial-erosion lakes dominate at both number (1478) and area (57.02 km^2) in the second classification system (Figure 7Figure 7), followed by end-moraine-dammed lakes and supraglacial lakes. Among the classified lakes, 137 are ice-contact lakes and cover an area of 5.56 km^2, implying a higher mean size of ice-contact lakes than supraglacial lakes.
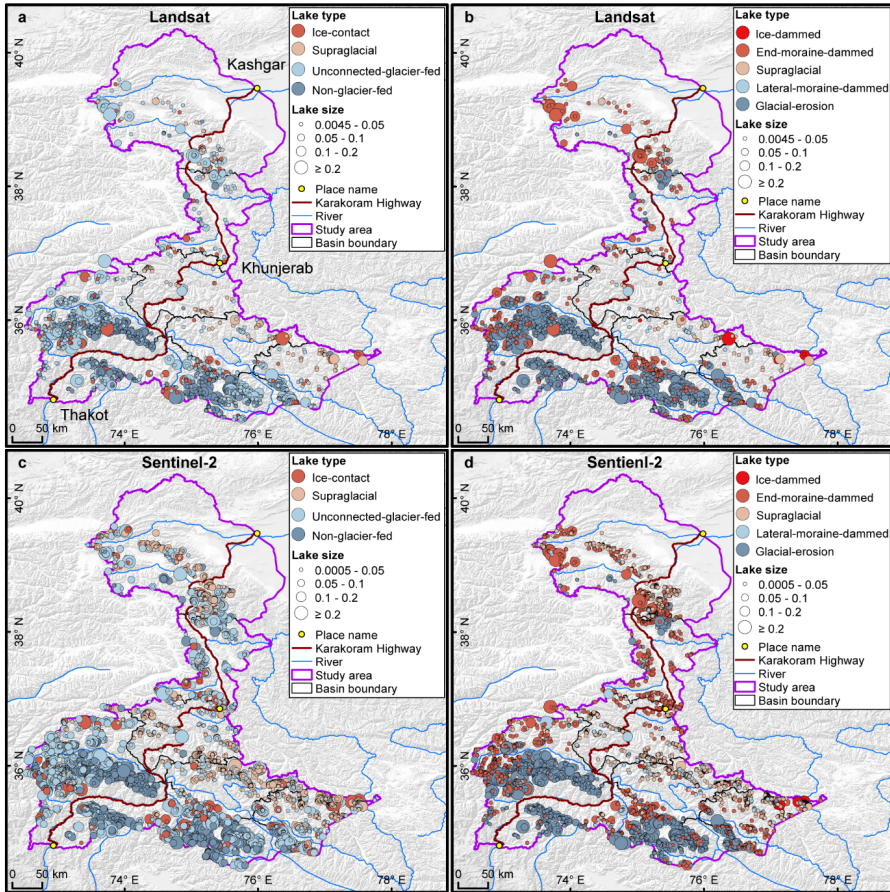
396
397 **Figure 5.** Distribution of glacial lakes in 2020 extracted from Landsat (a, b) and Sentinel-2 (c, d) images.
398 Panels a and c are classified by GLCS1, and GLCS2 for sub-graph b and d.
399
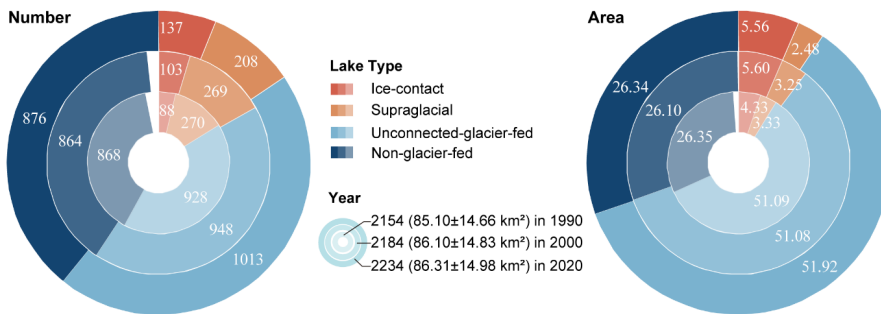
400
401 **Figure 6.** ~~Number~~ The number and area of different types of glacial lakes are classified based on the

402 condition of glacier supply in the study area (GLCS 1). The outermost ring represents glacial lake data in
403 2020, the middle ring for 2000, and the innermost ring for 1990. Lake number and area in 2020 were
404 selected as references, meaning a concept of "100 %" for a complete ring. Labeled values are scaled in
405 degrees rather than the radius of rings.
406
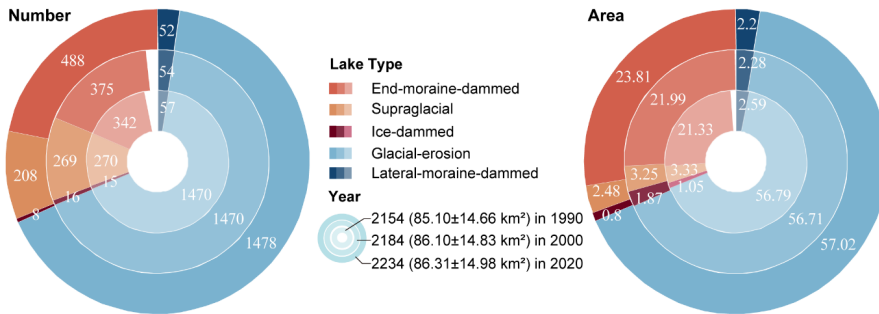
407
408 **Figure 7.** ~~Number~~ The number and area of different types of glacial lakes are classified based on glaciation
409 and the nature of the dam in the study area (GLCS 2). The outermost ring represents glacial lake data in
410 2020, the middle ring for 2000, and the innermost ring for 1990. Lake number and area in 2020 were selected
411 as references, meaning a concept of "100 %" for a complete ring. Labeled values are scaled in degrees rather
412 than the radius of rings.
413

414   The total number and area of glacial lakes in the study remain relatively stable with a
415 slight increase between 1990 and 2020, and the changes in count and area among various
416 types of glacial lakes vary substantially (Figure 6~~Figure 6~~ and Figure 7~~Figure 7~~). From 1990
417 to 2020, the total number of glacial lakes increased by 80 or 3.70%, while the area grew by
418 1.21 km^2 (or 1.42%). In GLCS1, unconnected-glacier-fed lakes have the largest increase in
419 number, followed by ice-contact and non-glacier-fed lakes, whereas supraglacial lakes
420 decreased by 62 in count. Ice-contact lakes expanded by 1.24 km^2 (equaling an increase of
421 26% in ice-contact lakes), ~~contributed~~ contributing ~~one~~ one-third of the total area increase.
422 Supraglacial lakes decreased by 0.85 km^2 in area whereas the areas of unconnected-glacier-
423 fed and non-glacier-fed lakes remained stable as a result of disconnections from glaciers
424 (Figure 6~~Figure 6~~). In GLCS2, end-moraine-dammed lakes increased by 2.48 km^2 and
425 contributed most of the glacier lake area expansion, whereas supraglacial, ice-dammed, and
426 lateral-moraine-dammed lakes decreased slightly in both number and area. Glacial-erosion
427 lakes accounted for the maximum percentage (about 66% for both count and area) in each
428 ~~time~~ period and remained stable (Figure 7~~Figure 7~~).

429 5.2 Glacier lake distribution observed from Sentinel-2

430 Sentinel-derived results ~~shows~~ show that there are 7,560 glacial lakes (103.70±8.45 km^2) in
431 2020 across the entire CPEC under an MMU of 5 pixels (500 m^2). Compared with Landsat-
432 derived product, glacial lakes from Sentinel-2 have similar spatial distribution characteristics
433 (Figure 5~~Figure 5~~); meanwhile, a larger quantity of glacier lakes, with more accurate
434 boundaries and a greater total lake area, were generated from Sentinel-2 images (Table

4Table 4). The smallest size class (0.0005-0.0045 km^2) contains the maximum lake number (4,969) but the least lake area (7.73±2.62 km^2), which is not available in the Landsat-derived lake data due to a coarser spatial resolution. In each size class, the overlap ratios are greater than 85% in count and area, and there are also a higher number and larger area of larger glacial lakes from Sentinel than that from Landsat images. Sentinel-2 images (10 m) with a finer spatial resolution produces more glacial lakes than thatthose from Landsat images (30 m). The discrepancy is mainly attributed to the inconsistency of spatial resolutions and image acquisition dates, more being as discussed in the section 6.2..

Table 4. Count and area of glacial lakes mapped from Sentinel-2 and Landsat images in 2020 in various size classes.

Lake size km^2	Glacial lakes from Sentinel-2 count (km^2)	Glacial lakes from Landsat count (km^2)	Overlap % (%)
0.0045-0.05	2182 (35.52±3.72)	1870 (31.47±9.57)	85.70 (88.60)
0.05-0.1	237 (16.37±0.89)	204 (14.07±2.18)	86.08 (85.95)
0.1-0.2	122 (16.88±0.68)	115 (15.91±1.83)	94.26 (94.25)
≥0.2	50 (27.20±0.54)	45 (24.86±1.40)	90.00 (91.40)
Total	2591 (95.97±5.83)	2234 (86.31±14.98)	86.22 (89.93)

Note: Second column excludes 4969 (7.73±2.62 km^2) lakes in the 0.0005 to 0.0045 km^2 range. Overlap % (%) represents the ratios between our Landsat-derived dataset and Sentinel-derived product in count and area, respectively.

6 Discussions

6.1 Uncertainty and error of lake mapping

The uncertainty estimated from our improved equation shows that the relative error of individual glacial lakes decreases when lake size increases or the cell size of remote sensing images reduces (Lyons et al., 2013; Carrivick and Quincey, 2014) (Figure 8Figure 8). Total area errors of glacial lakes in the study area are approximate ±14.98 km^2 and ±8.45 km^2 in 2020 for Landsat and Sentinel-2 datasets, respectively, and the average relative errors are ±17.36% and ±8.15%. Generally, small lakes have greater relative errors. For example, the mean relative error is 35.38% for Landsat Landsat-derived glacial lakes between 0.0045 and 0.1 km^2 and 10.63% for glacial lakes greater than 0.1 km^2. The mean area error of Sentinel-derived glacial lakes is almost one one-third of that extracted from Landsat images for glacial lakes of all or specific size groups. Because the relative error was estimated as a function of satellite image spatial resolution and lake perimeter, the calculated error for a large lake is proportionally smaller than that of a small lake (Salerno et al., 2012) and the error for Landsat-derived lake is naturally greater than that of Sentinel-derived lake at the same size group.

带格式的: 字体: 非加粗

465

466
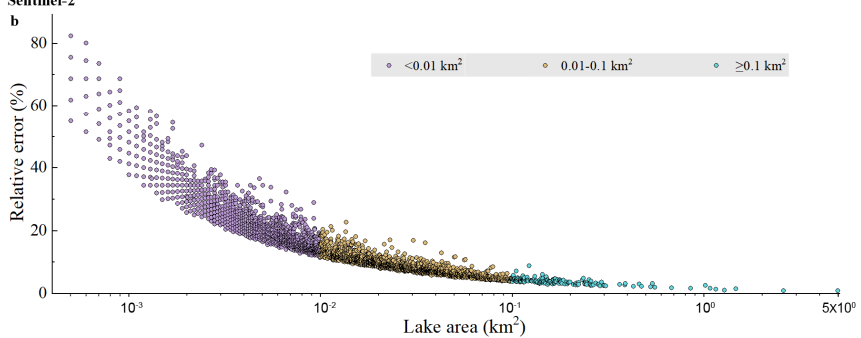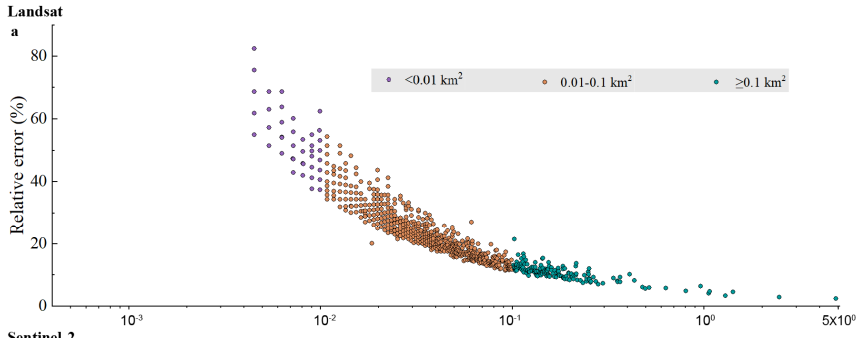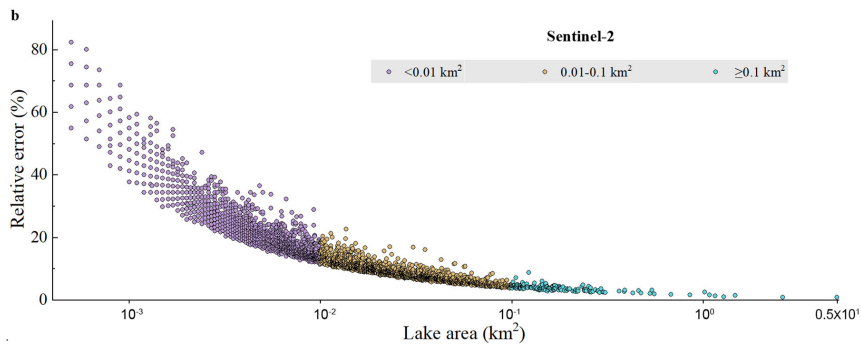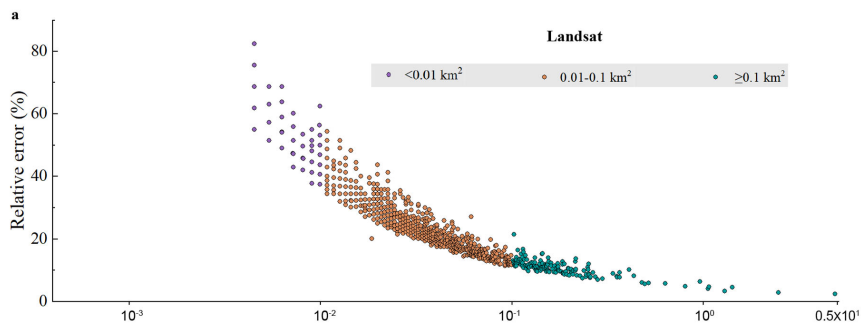
Figure 8. ~~Estimated~~ The estimated relative error for glacial lakes of all or specific size ranges in the study area. Error estimation is based on the modified equation and lake data extracted from Landsat (a) and Sentinel-2 images (b).

Our Landsat- and Sentinel-derived glacial lake dataset match well lake boundaries in Google Earth higher resolution images (Figure 9~~Figure 9~~). The mean difference in area is 0.005 km² between Landsat- and Google ~~Earth~~ Earth-derived lakes and 0.001 km² between Sentinel-~~2~~ and Google ~~Earth~~ Earth-derived lakes, and major validation samples (84/89) are within the confidence interval of 95%, indicating ~~a~~ high accuracy in lake mapping (Figure 9~~Figure 9~~c and d). The error of 89 sample lakes is 5.48% in the total area between Landsat- and Google Earth-derived data, and 0.61% for Sentinel- and Google Earth-derived data. The median (±standard deviation) in a discrepancy of the individual lake area is 7.66±4.96 % for Landsat- and Google Earth-derived data, and 4.46±4.62 % for Sentinel- and Google Earth-derived data. Our glacial lake dataset shows ~~a~~ satisfactory mapping accuracy, although Sentinel-derived lake data performs more accurate_ly_ than those from Landsat images. We also validated the sampling of Landsat-derived 89 lakes by the existing Landsat-extracted lake data produced by Wang et al. (2020). A total of 83 lakes are available in Wang's data with a mean difference of 0.005 km² in the lake area (Figure A8). This also shows an improvement ~~of~~ in our lake product in contrast to the existing dataset.
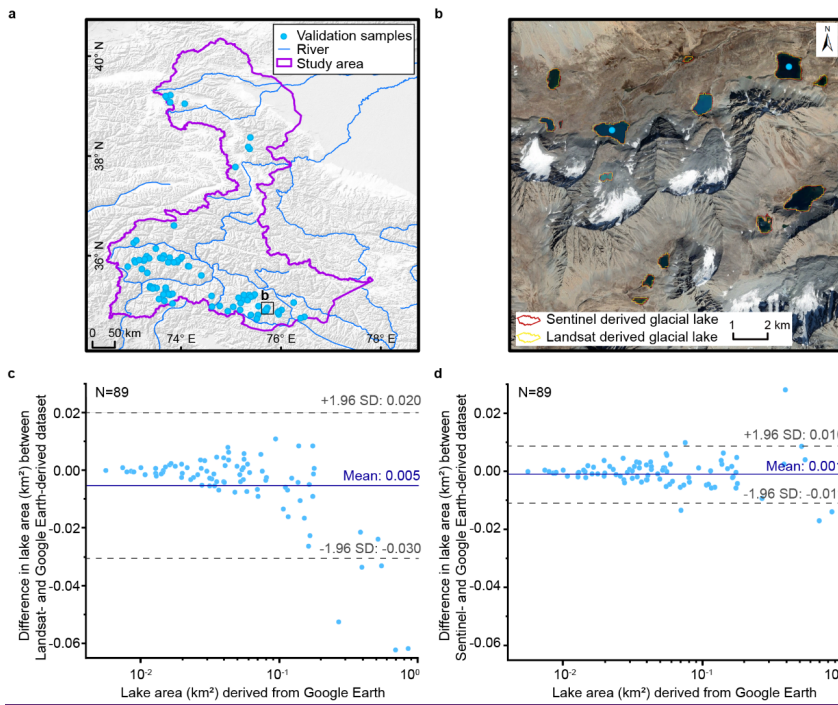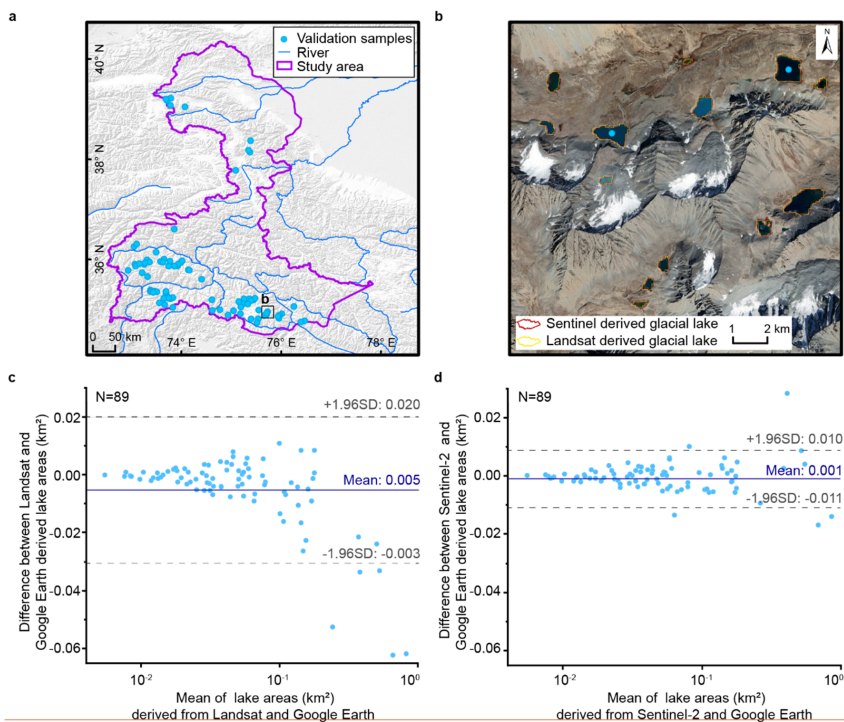
Figure 9. Distribution of the validation sample (a), visual comparison of glacial lakes derived from Landsat and Sentinel-2 images overlaying Google Earth imagery (© Google Earth 2019) in a zoomed site (b), and differences between our glacial lake product (mapped from Landsat and Sentinel-2 images) and the validation reference (digitized from Google Earth images) (c and d).

6.2 Comparison of Sentinel-2 and Landsat-–derived products

Glacial lakes from Landsat and Sentinel-2 images have a high consistency in number and area with overlap rates from approximately 86% to 94% for all lakes greater than 0.0045 km^2 (Table 4Table 4), indicating a good potential for coordinated utility with Landsat archived observation (Figure 10Figure 10). Lake extents extracted from Landsat and Sentinel images match well for various types and sizes (Figure 10Figure 10 and Figure 11Figure 11, Table 4Table 4). The best consistency rate reaches 94% for the glacial lakes between 0.1 km^2 and 0.2 km^2. The difference in the area of glacial lakes extracted from Landsat and Sentinel-2 images generally liess within the uncertainty ranges.

Landsat derived glacial lake   Sentinel derived glacial lake   0   400m
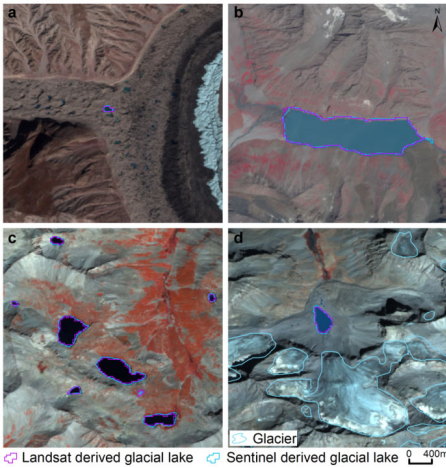
Figure 10. High consistency of lake extents extracted from Landsat and Sentinel-2 images. Lake types shown include supraglacial (a), glacier-fed moraine-dammed (b), unconnected glacial-erosion lake without glacier melt supply (c), and glacier-fed moraine-dammed lakes (d).

~~Spatial~~ The spatial resolution of satellite images plays a primary role in the discrepancies in count and area of glacial lakes extracted from Landsat (30 m) and Sentinel-2 (10 m) observations. Due to a finer spatial resolution, Sentinel-2 images can extract more glacial lakes and more accurate extents than those from Landsat images. We set the same 5 pixels as the MMU for both Landsat and Sentinel-2 images, which corresponds to a minimum area of 0.0045 km^2 and 0.0005 km^2, respectively. The minimum mapping area results in generating nearly 5000 more lakes from Sentinel-2 images than from Landsat images, causing the greatest discrepancy in number ~~(Table 4)~~, such as Figure 11~~Figure 11~~a. Small lakes such as supraglacial lakes play an important role in analyzing glacier evolution and supraglacial drainage systems (Liu and Mayer, 2015; Miles et al., 2018), implying a potential of our dataset to be applied in studies of glacier-lake evolutions. Meanwhile, Sentinel-2 images ~~are able to~~can depict boundaries of glacial lakes with ~~a~~ lower uncertainty, as ~~for~~ some small islands and narrow channels (Figure 11~~Figure 11~~b and c) were mapped from Sentinel-2 imagery that ~~were~~ was unable to be detected in Landsat imagery.

In addition to the difference in image resolution, different acquisition dates between Sentinel-2 and Landsat images can also contribute to the discrepancy ~~of~~ between those two glacial lake datasets. The total number of S~~s~~upraglacial lakes and ice-dammed glacial lakes are less than 300, but those lakes are controlled by glacier movement and temperature changes (Liu and Mayer, 2015; Miles et al., 2018), ~~and~~which vary faster with time than relatively stable glacial-erosion and moraine-dammed lakes. Acquiring same-day images from the two sensors ~~were~~ was not always possible due to the impacts of cloud contaminations, topographic shadows, snow cover, and revisit periods (Williamson et al., 2018; Paul et al., 2020). Despite our efforts of leveraging all available high-quality images,

530 the overlap of acquisition dates between Landsat and Sentinel-2 images for the same location
531 is relatively low (only 7 scenes of Sentinel-2 images or 112 glacial lakes in 2020) in this
532 study area, and the consequential temporal gaps led to a difference in the number and area of
533 the derived glacial lakes. As exemplified in Figure 11Figure 11d, the mapped supraglacial
534 lakes in the same areas exhibitlocation exhibit a substantial considerable discrepancy, which
535 is likely a joint consequence of both sensor difference and actual glacier lake dynamics
536 evolutionthat occurred during this short period of time. Despite our efforts of leveraging all
537 available high-quality images, the overlap of acquisition dates between Landsat and Sentinel-
538 2 images for the same location is relatively low (only 7 scenes of Sentinel-2 images or 112
539 glacial lakes in 2020) in this study area, and the consequential temporal gaps led to a
540 difference in the number and area of the derived glacial lakes.
541
542

带格式的: 字体: (中文) Times New Roman, 非加粗

带格式的: 字体颜色: 文字 1
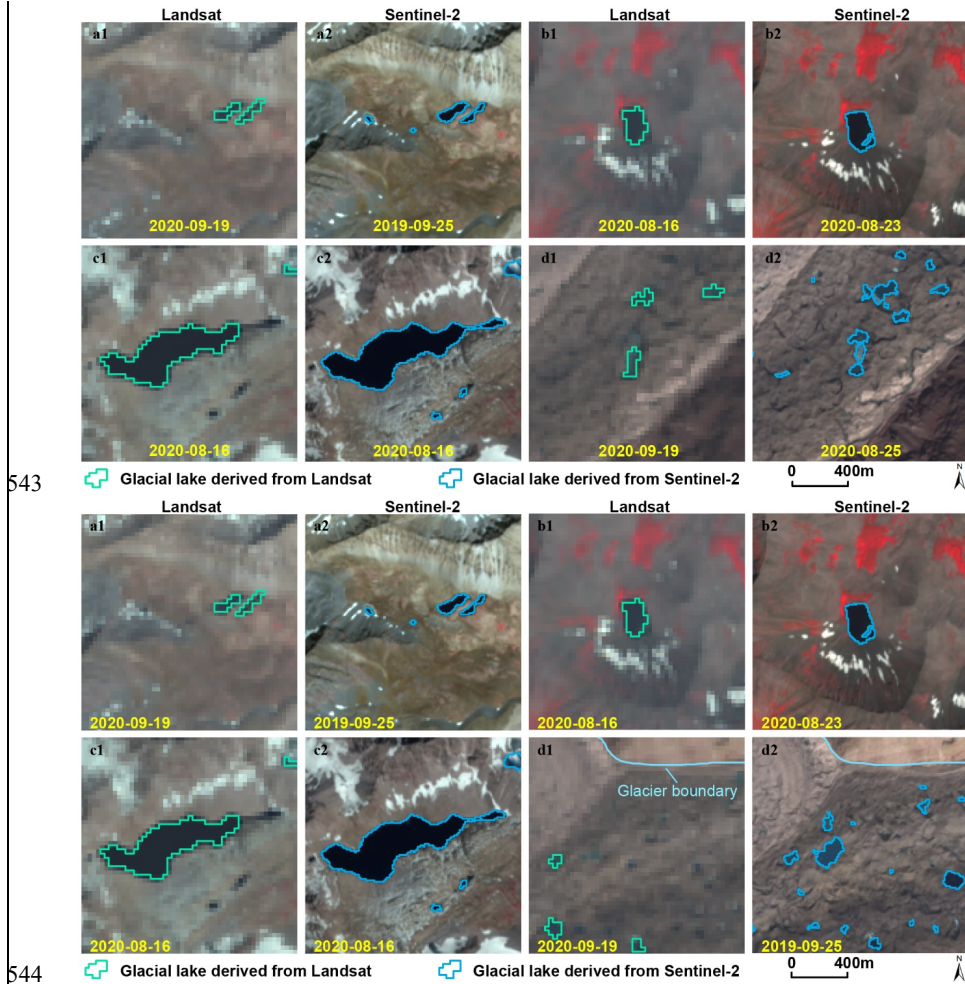
Figure 11. ~~Discrepancy~~ The discrepancy of lake extents extracted from Landsat and Sentinel-2 images.

6.3 Comparison with the previous similar dataset

An increasing number of glacier lake datasets have been released over the past years, and most of them were produced from long-term Landsat archives. Regional glacial lake datasets using Sentinel images are scarce. ~~Lack~~ The lack of Sentinel-derived glacial lake data in the study area makes it impossible to compare. Here we selected four available glacial lake datasets to compare with our Landsat-derived dataset at the same MMU and study area.

We provide the latest glacial lake dataset (in 2020) and the most long-term 30-m Landsat observation (1990 to 2020) for this study, with a range of critical attributes including two types of classification systems. Within the same study area, our 2020 glacial lakes appear to

be closest to the 2018 dataset produced by Wang et al. (2020), with the highest overlap of greater than 91% in count at the minimum mapping unit of 5400 m^2 or 6 pixels (Table 5~~Table 5~~). ~~In~~ Wang's dataset ~~et al.~~ (2020) ~~, the minimum mapping unit is 6 pixels so their dataset has a less lake quantity. However, their dataset~~ contains many large landslide-dammed lakes that are excluded in our glacial lake mapping. ~~As a result~~, so their total glacier lake area is greater than ours.

The overlapping rates between Wang's glacial lakes (2020) in 1990 and ours are more than ~~838~~583% in count. However, their results show a distinct increase of glacial lakes in number and area between 1990 and 2018 (Wang et al., 2020) whereas our data show a more stable change between 1990 and 2020. One possible reason is that manually delineating glacial lakes twice by different operators during Wang's lake mapping (2020) exacerbates the errors of mapping. Another reason is that their data contains landslide-dammed lakes that fluctuate greatly with time and expanded recently. One example is ~~the~~ Attabad Lake (Located at 36°18'22.33"N, 74°49'34.36"E).

Table 5. Comparison between our Landsat-based mapping and other third-party Landsat-based glacial lake datasets in the study area.

Baseline year (them/us)	Method (them/us)	MMU m^2 (pixels)	Count (them)	Count (us)	Ratio (%)	Reference
1990/1990	Manual/Semi-automated	5400 (6)	1720	2069	83.13	Wang et al., 2020
1990/1990	Automated/Semi-automated	50000 (55)	145	363	39.94	Shugar et al., 2020
1990/1990	Manual/Semi-automated	4500 (5)*	622	2154	28.88	Zhang et al., 2015
2000/2000	Manual/Semi-automated	4500 (5)*	724	2184	33.15	Zhang et al., 2015
2000/2000	Automated/Semi-automated	50000 (55)	155	361	42.94	Shugar et al., 2020
2008/2000	Automated & Manual/Semi-automated	8100 (9)	1067	1800	59.28	Chen et al., 2021
2015/2020	Automated/Semi-automated	50000 (55)	148	364	40.66	Shugar et al., 2020
2017/2020	Automated & Manual/Semi-automated	8100 (9)	1063	1813	58.63	Chen et al., 2021
2018/2020	Manual/Semi-automated	5400 (6)	1956	2149	91.02	Wang et al., 2020

Baseline year (period)	Method	MMU m² (pixels)	Count (km²)	Other data / our product % (%)	Reference
1990 (1988-1993)	Manual	5400 (6)	1720 (89.68±13.69)	83.13 (105.87)	Wang et al., 2020
1990 (1989-1994)	Semi-automated	5400 (6)	2069 (81.71±14.41)		This study
1990 (1990-1999)	Automated	50000 (55)	145 (20.28)	38.77 (36.98)	Shugar et al., 2020
1990 (1989-1994)	Semi-automated	50000 (55)	374 (54.84±5.49)		This study
1990 (1989-1992)	Manual	4500 (5)*	622 (51.93±10.15)	28.88 (61.02)	Zhang et al., 2015
1990 (1989-1994)	Semi-automated	4500 (5)*	2154 (85.10±14.66)		This study
2000 (1999-2001)	Manual	4500 (5)*	724 (61.41±11.91)	33.15 (71.32)	Zhang et al., 2015
2000 (1996-2004)	Semi-automated	4500 (5)*	2184 (86.10±14.83)		This study
2000 (2000-2004)	Automated	50000 (55)	155 (22.35)	42.94 (40.70)	Shugar et al., 2020
2000 (1996-2004)	Semi-automated	50000 (55)	361 (54.91±5.40)		This study
2008	Automated & Manual	8100 (9)	1067 (65.45)	59.28 (78.08)	Chen et al., 2021
2000 (1996-2004)	Semi-automated	8100 (9)	1800 (83.82±13.59)		This study
2015 (2015-2018)	Automated	50000 (55)	148 (21.45)	40.66 (39.11)	Shugar et al., 2020
2020 (2016-2020)	Semi-automated	50000 (55)	361 (54.84±5.41)		This study
2017	Automated & Manual	8100 (9)	1063 (63.23)	58.63 (75.45)	Chen et al., 2021

2020 (2016-2020)	Semi-automated	8100 (9)	1813 (83.80±13.63)		This study
2018 (2017-2018)	Manual	5400 (6)	1956 (102.46±15.48)	91.02 (119.24)	Wang et al., 2020
2020 (2016-2020)	Semi-automated	5400 (6)	2149 (85.93±14.74)		This study

Note: MMU represents the minimum mapping unit that is possible to enable a valid comparison between our product and each of the third-party datasets. * The MMU in the dataset of Zhang et al. (2015) is 3 pixels, finer than 5 pixels in our product, so an MMU threshold of 5 pixels was used for this comparison. "% (%)" represents the ratios between the third-party dataset and our product in count and area, respectively.

The second highest overlapping rate is approximate 59% for 2008 and 58% for 2017 in count comparing with Chen's data (Chen et al., 2021). Similarly, a minimum mapping unit of 55 pixels (50000 m²) in the overlapping rate between Shugar et al.'s, dataset (2020) and ours is is led to lower overlap with less than 43% in count and area at the minimum mapping unit of 50000 m². The dataset from Zhang et al. (2015) shows fewer glacial lakes in 1990 and 2000 even with a smaller at the same MMU of 53 pixels. Our product has more lakes than each of the other 4 products at 9 time periods. By inspecting their dataset, we attributed this anomalous discrepancy to a range of glacial lakes that were missing due to a lack of thorough cross-check quality assurance during their manual delineation lake mapping over a larger study area. And those more glacial lakes show an improvement of our product in contrast to the previous similar datasets. Our Landsat Landsat-derived glacial lake dataset has been visually cross-checked over three time periods after the step of threshold-based semi-automated lake mapping, and has also been visually validated by Sentinel-2 derived glacial lakes. Through this series of quality assurance, we aim at delivering one of the most reliable multi-decadal glacial lake products for this study area.

Other factors, such as image quality and acquisition dates, mapping methods, and quality assurance workflow, might also lead to the discrepancies between the glacial lake datasets. Despite such discrepancies, an increasing number of publically-shared datasets benefit potential users to select the most suitable one for their objectives. Herein, we provide an up-to-date glacial lake dataset derived from both Landsat and Sentinel-2 observations, which further increased the availability of glacial lake dataset for water resource and GLOFs risk assessment, predicting glacier-lake evolutions (Carrivick et al., 2020) in the context of climate change.

6.4 Limitation and updating plan

We would like to acknowledge several limitations of our glacier lake dataset, largely due to the availability of high high-quality satellite images in the study area and inadequate field survey data (Wang et al., 2020; Chen et al., 2021). First, it is unlikely to collect enough good-quality images within one calendar year for the entire study area due to the high possibility of cloud or snow covers. Even though the capacity of repeat observations for Landsat-8 OLI and Sentinel-2 increased (Roy et al., 2014; Williamson et al., 2018; Wulder et al., 2019; Paul et al., 2020), the 2020 glacial lake dataset has to employ images acquired in adjacent years besides 2020. Most images used from Landsat and Sentinel-2 platforms were imaged in autumn, and some images taken between April and July and in November also were employed. Distribution and changes in glacial lakes primarily represent the characteristics between August and October. Glacial lakes evolve with time and space (Nie et al., 2017), and

subtle inter- and intra-annual changes (Liu et al., 2020) for each ~~time~~ period were ignored. Second, field investigation data are limited due to the low accessibility of the high mountain environment in the study area, which restrained the accuracy in classifying the glacial lake types. Although very high-resolution Google Earth images were utilized to assist in ~~lake~~ lake-type interpretation, occasional misclassification was unavoidable. We implemented two types of classification systems based on a careful utilization of glacier data, DEM, geomorphological features, and expert knowledge. However, the lack of in situ surveys prohibited a thorough validation of the glacial lake types. Third, the rigorous quality assurance and ~~cross~~ cross-check after semi-automated lake mapping assures the quality of our lake dataset but are still time and ~~cost~~ cost-prohibitive. State-of-the-art mapping methods, such as deep learning method (Wu et al., 2020), Google Earth Engine cloud-computing (Chen et al., 2021), and synergy of SAR and optical images (Wangchuk and Bolch, 2020; How et al., 2021), would be used in the future to balance product accuracy and time cost.

The glacial lake dataset will be updated using newly collected Landsat and Sentinel images at a five-year interval or modified according to user feedbacks. The updated glacial lake dataset will continue to be released freely and publicly on the Mountain Science Data Center sharing platform.

7 Data availability

Our glacial lake dataset extracted from Sentinel-2 images in 2020 and Landsat observation between 1990 and 2020 are available online via the Mountain Science Data Center, the Institute of Mountain Hazards and Environment, the Chinese Academy of Sciences at https://doi.org/10.12380/Glaci.msdc.000001 (Lesi et al., 2022). The glacial lake dataset is provided in both ESRI shapefile format (total size of 22.6 MB) and the Geopackage format (version 1.2.1) with a total size of 9.2MB, which can be opened and further processed by open-source geographic information system software such as QGIS.

8 Conclusions

Glacial lake inventories of the entire China-Pakistan Economic Corridor in 2020 were provided based on Landsat and Sentinel-2 images using a threshold-based semi-automated mapping method. Both Landsat and Sentinel-2 derived glacial lake dataset show similar characteristics in spatial distribution and ~~in~~ the statistics of count and area. By contrast, the glacial lake dataset derived from Sentinel-2 images with a spatial resolution of 10 m has a lower mapping error and more accurate lake boundary than those from 30 m spatial resolution Landsat images whereas Landsat imagery is more suitable to analyze spatial-temporal changes at a longer time scale due to its long-term archived observations at a consistent 30 m spatial resolution starting from the late 1980s.

Glacial lakes in the study area remain relatively stable with a slight increase in number and area between 1990 and 2020 according to Landsat observations. Our dataset reveals that 2154 glacial lakes in 1990 covering 85.1 ± 14.66 km^2 increased to 2234 lakes with a total area of 86.31 ± 14.98 km^2. The same mapping method and rigorous workflow of quality assurance and quality control used in this study reduced the error in multi-temporal changes of glacial lakes.

The Hanshaw's error estimation method for pixel-based lake mapping was improved by removing repeatedly calculated edge pixels that vary with lake shape. Therefore, the newly proposed method reduces the estimated value of uncertainty from satellite observations. The average relative error is ±17.36% for the Landsat-derived product dataset and ±8.15% for the product from Sentinel-2.

Our glacial lake dataset contains a range of critical parameters that maximize their potential utility for water resource and GLOFs risk evaluation, cryosphere-hydrological, and glacier-lake evolution projection. The dual classification systems of glacial lake types were developed and are very likely to attract broader researchers and scientists to use our datasets. In comparison with other existing glacial lake datasets, our products were created through a thorough consideration of lake types, cross cross-checks, and rigorous quality assurance, and will be updated and released continuously in the Mountain Science Data Center. As such, we expect that our glacial lake dataset will have significant value to cryospheric-hydrology research, the assessment of water resources, and glacier-related hazards in the CPEC.

Appendix. The appendix related to this article is available online.

Author contributions. ML and YN conceived the study, ML, YN and XD performed data processing and analysis of the glacial lake inventory data, JW contributed to tool development and mapping methods, and ML and YN wrote the manuscript. All authors reviewed and edited the manuscript before submission.

Competing interests. The authors declare no conflict of interest.

Acknowledgements.
We are grateful for to the chief editor (ice) Kenneth Mankoff and three anonymous referees for their constructive comments that greatly help us to improve this manuscript. This study was supported by the second Tibetan Plateau Scientific Expedition and Research Program (grant 2019QZKK0603), the National Natural Science Foundation of China (Grant Nos. 42171086, 41971153), the International Science & Technology Cooperation Program of China (No. 2018YFE0100100), the Chinese Academy of Sciences "Light of West China" and Natural Sciences and Engineering Research Council of Canada (Grant No. DG-2020-04207).

Appendix

Tutorial for Improved Uncertainty Estimating Method

~~The~~ Hanshaw's equation was originally proposed for pixelated polygons (such as a polygon directly extracted from a remote sensing image), and performed more robustly than manually digitized polygons (where vertices do not necessarily follow the pixel edges). Our improved method also performs better for pixelated polygons. This tutorial is dedicated to helping implement our improved uncertainty estimation method.

~~Procedure~~ The procedure of uncertainty estimating method (using ArcGIS (© ESRI) for example)

1. Removing redundant nodes (optional)

We found that a small proportion (~1%) of the pixelated lake polygons (directly extracted from satellite images) have redundant nodes, which affects the value of inner nodes. If no redundant nodes exist, this step can be skipped. Or, we recommend using the "Simplify Polygon" tool in ArcGIS to remove those nodes (Figure A1~~Figure A1~~).

    In the Simplify Polygon panel

- Input your dataset.
- Set the output path and output file name.
- Choose the simplification algorithm. We recommended "POINT_REMOVE".
- Set the tolerance of the simplification algorithm. In this step, we need to ensure that the polygon boundaries remain unchanged after deleting redundant nodes. Generally, a tolerance of 1 meter will suffice, or you can adjust the threshold until your satisfaction.
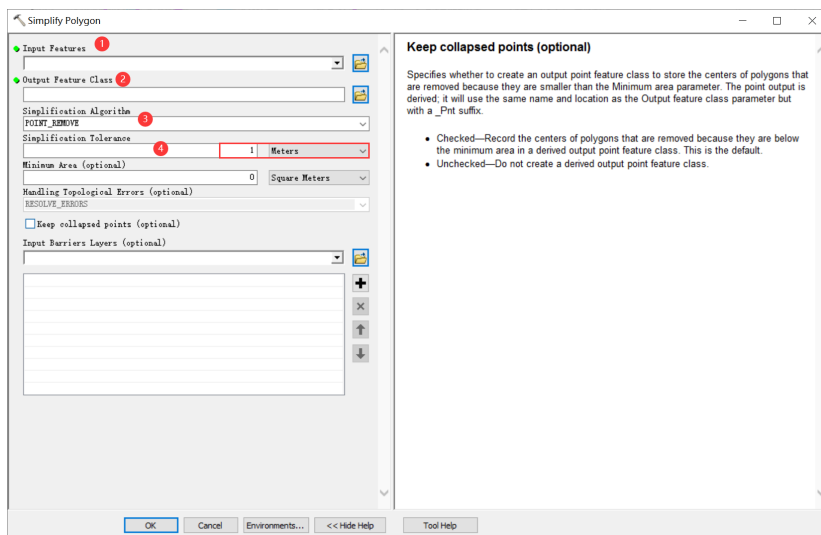
Figure A1. Input and option for Simplify Polygon in ArcGIS.

717

718 2. Calculating the total number of nodes using ArcGIS (Figure A2~~Figure A2~~):

719 ● Add a new field in the attribute table of the dataset.

720 ● Open Field Calculator.

721 ● Switch the parser to ~~python~~ python- mode, and enter the following code

722 "!shape.pointcount!" in the blue box to calculate the total number of nodes for each

723 glacial lake boundary.

724
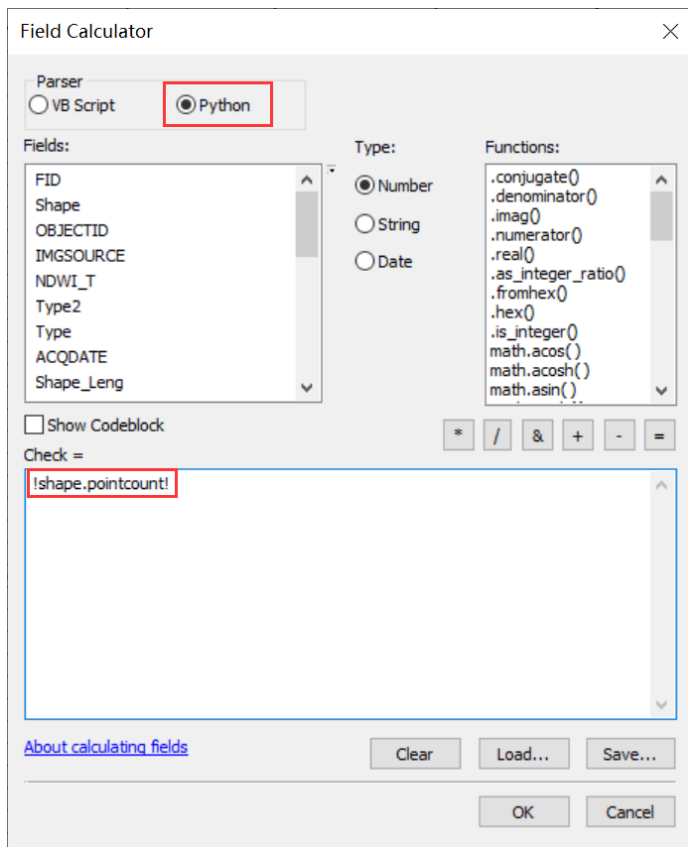
725 **Figure A2.** Total node calculation in ArcGIS.

726

727 3. Calculating the number of inner nodes:

728

729 For polygons without islands (Figure A3~~Figure A3~~), use ~~the~~ equation 5. An inner node is a

730 polygon vertex where the interior angle surrounding it is greater than 180 degrees. An outer

731 node is the opposite of the inner node, where the interior angle is less than 180 degrees. We

732 found that the outer nodes are usually four more than the inner nodes in our glacial lake

733 dataset. The total nodes in ArcGIS contain one overlapping node to close the polygon,

734 meaning the endpoint is also the start point. This extra count was deleted ~~in~~ from the
735 calculation (equation 5).
736
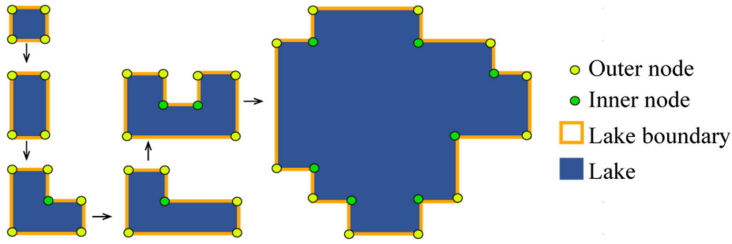
738 **Figure A3.** Sketch of outer and inner nodes of various glacial lakes without island.
739

740 For polygons with island~~s~~ (Figure A4~~Figure A4~~) use ~~the~~ equation 6.

741
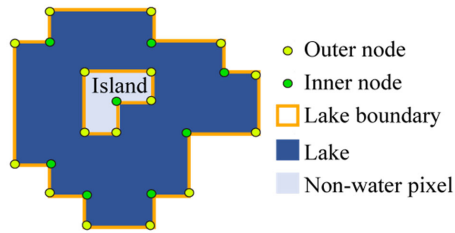
742
743 **Figure A4.** Sketch of outer and inner nodes for a glacial lake with an island.
744

745 We further specify the steps below to help implement equation 6.
746

747 Sept 1: detect the number of islands within each polygon.
748 ● Convert the initial lake polygon to a polyline using the "Feature To Line" tool (Figure

749 A5~~Figure A5~~).
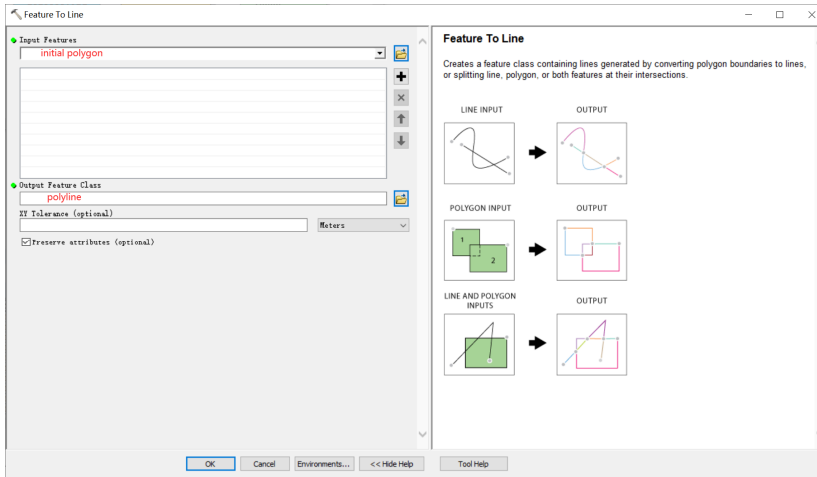
750
751 **Figure A5.** Feature To Line tool in ArcGIS
752
753 ● Convert the polyline to generate a new polygon (Figure A6Figure A6).
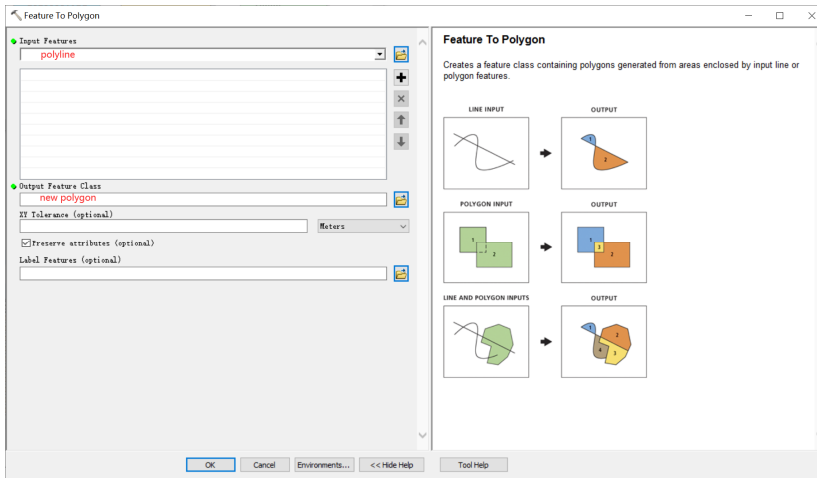
754
755 **Figure A6.** Feature To Polygon tool in ArcGIS
756
757 ● Erase the new polygon by the initial polygon, which outputs the islands. Then we can
758 count how many islands there are in each lake (Figure A7Figure A7).
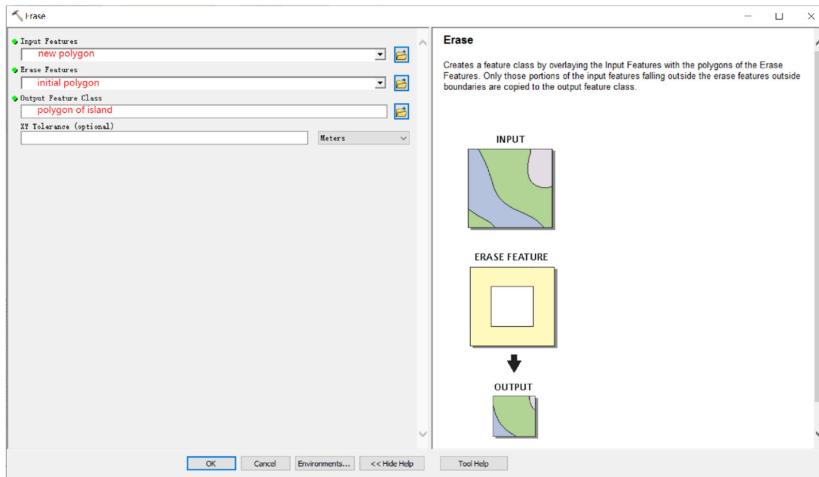
759
760   **Figure A7.** Erase tool in ArcGIS.
761
762   Step 2: calculate the number of inner nodes for each polygon with an island or islands using
763   equation 6.
764
765   4. Calculating the uncertainty of lake mapping using equation 4.
766
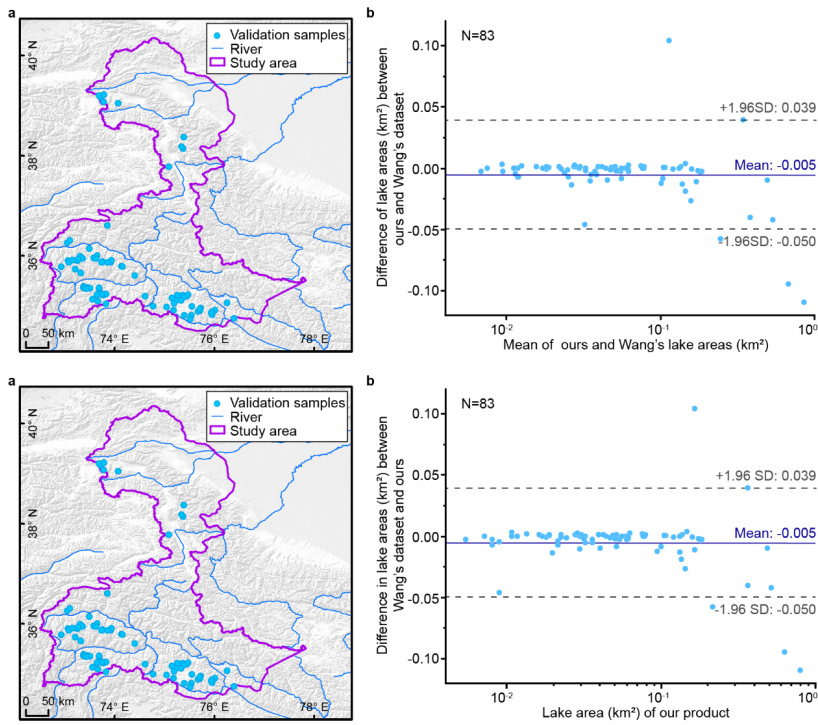
Figure A8. Distribution of validation samples (a) and comparison of glacial lakes (b) derived from our Landsat product in 2020 and Wang's lake data in 2018.

References:

[1]. Lesi, M., et al., Landsat and Sentinel-derived glacial lake dataset in the China-Pakistan Economic Corridor from 1990 to 2020. Mountain Science Data Center, 2022.

[2]. Wang, X., S. Liu and J. Zhang, A new look at roles of the cryosphere in sustainable development. Advances in Climate Change Research, 2019. 10(2): p. 124-131.

[3]. Viviroli, D., et al., Increasing dependence of lowland populations on mountain water resources. Nature Sustainability, 2020. 3(11): p. 917-928.

[4]. Pritchard, H.D., Asia's shrinking glaciers protect large populations from drought stress. Nature, 2019. 569(7758): p. 649-654.

[5]. Nie, Y., et al., Glacial change and hydrological implications in the Himalaya and Karakoram. Nature Reviews Earth & Environment, 2021. 2(2): p. 91-106.

[6]. Brun, F., et al., A spatially resolved estimate of High Mountain Asia glacier mass balances from 2000 to 2016. Nature Geoscience, 2017. 10(9): p. 668-673.

[7]. Shean, D.E., et al., A Systematic, Regional Assessment of High Mountain Asia Glacier Mass Balance. Frontiers in Earth Science, 2020. 7: p. 363.

[8]. Bhattacharya, A., et al., High Mountain Asian glacier response to climate revealed by multi-temporal satellite

observations since the 1960s. Nature Communications, 2021. 12(1): p. 4133.

[9]. Maurer, J.M., et al., Acceleration of ice loss across the Himalayas over the past 40 years. Science Advances, 2019. 5(6): p. eaav7266.

[10]. Huss, M. and R. Hock, Global-scale hydrological response to future glacier mass loss. Nature Climate Change, 2018. 8(2): p. 135-140.

[11]. Carrivick, J.L. and F.S. Tweed, A global assessment of the societal impacts of glacier outburst floods. Global and Planetary Change, 2016. 144: p. 1-16.

[12]. Nie, Y., et al., An inventory of historical glacial lake outburst floods in the Himalayas based on remote sensing observations and geomorphological analysis. Geomorphology, 2018. 308: p. 91-106.

[13]. Zheng, G., et al., Increasing risk of glacial lake outburst floods from future Third Pole deglaciation. Nature Climate Change, 2021. 11(5): p. 411-417.

[14]. Rounce, D.R., R. Hock and D.E. Shean, Glacier Mass Change in High Mountain Asia Through 2100 Using the Open-Source Python Glacier Evolution Model (PyGEM). Frontiers in Earth Science, 2020. 7: p. 331.

[15]. Shugar, D.H., et al., A massive rock and ice avalanche caused the 2021 disaster at Chamoli, Indian Himalaya. Science, 2021. 373(6552): p. 300-306.

[16]. Shugar, D.H., et al., Rapid worldwide growth of glacial lakes since 1990. Nature Climate Change, 2020. 10(10): p. 939-945.

[17]. Immerzeel, W.W., et al., Importance and vulnerability of the world's water towers. Nature, 2020. 577(7790): p. 364-369.

[18]. Carrivick, J.L., et al., Ice-Marginal Proglacial Lakes Across Greenland: Present Status and a Possible Future. Geophysical Research Letters, 2022. 49(12): p. e2022GL099276.

[19]. Li, Z., X. Deng and Y. Zhang, Evaluation and convergence analysis of socio-economic vulnerability to natural hazards of Belt and Road Initiative countries. Journal of Cleaner Production, 2021. 282(125406): p. 125406.

[20]. Battamo, A.Y., et al., Mapping socio-ecological resilience along the seven economic corridors of the Belt and Road Initiative. Journal of Cleaner Production, 2021. 309(127341): p. 127341.

[21].Hewitt, K., Glaciers of the Karakoram Himalaya: Glacial Environments, Processes, Hazards and Resources. 2014, Dordrecht: Springer.

[22]. Bhambri, R., et al., Ice-dams, outburst floods, and movement heterogeneity of glaciers, Karakoram. Global and Planetary Change, 2019. 180(9): p. 100-116.

[23]. Wang, X., et al., Glacial lake inventory of high-mountain Asia in 1990 and 2018 derived from Landsat images. Earth System Science Data, 2020. 12(3): p. 2169-2182.

[24]. Nie, Y., et al., A regional-scale assessment of Himalayan glacial lake changes using satellite observations from 1990 to 2015. Remote Sensing of Environment, 2017. 189(2): p. 1-13.

[25]. Brun, F., et al., Heterogeneous Influence of Glacier Morphology on the Mass Balance Variability in High Mountain Asia. Journal of Geophysical Research: Earth Surface, 2019. 124(6): p. 1331-1345.

[26]. Liu, Q., et al., Interannual flow dynamics driven by frontal retreat of a lake-terminating glacier in the Chinese Central Himalaya. Earth and Planetary Science Letters, 2020. 546: p. 116450.

[27]. Carrivick, J.L., et al., Toward Numerical Modeling of Interactions Between Ice-Marginal Proglacial Lakes and Glaciers. Frontiers in Earth Science, 2020. 8.

[28]. Huggel, C., et al., Remote sensing based assessment of hazards from glacier lake outbursts: a case study in the Swiss Alps. Canadian Geotechnical Journal, 2002. 39(2): p. 316-330.

[29]. Quincey, D.J., et al., Early recognition of glacial lake hazards in the Himalaya using remote sensing datasets. Global and Planetary Change, 2007. 56(1-2): p. 137-152.

832 [30]. Zhang, G., et al., An inventory of glacial lakes in the Third Pole region and their changes in response to
833 global warming. Global and Planetary Change, 2015. 131: p. 148-157.
834 [31]. Gardelle, J., Y. Arnaud and E. Berthier, Contrasted evolution of glacial lakes along the Hindu Kush Himalaya
835 mountain range between 1990 and 2009. Global and Planetary Change, 2011. 75(1-2): p. 47-55.
836 [32]. Chen, F., et al., Annual 30 m dataset for glacial lakes in High Mountain Asia from 2008 to 2017. Earth
837 System Science Data, 2021. 13(2): p. 741-766.
838 [33]. Wang, X., et al., Changes of glacial lakes and implications in Tian Shan, Central Asia, based on remote
839 sensing data from 1990 to 2010. Environmental research letters, 2013. 8(4): p. 44052.
840 [34]. Rick, B., et al., Dam type and lake location characterize ice-marginal lake area change in Alaska and
841 NW Canada between 1984 and 2019. The Cryosphere, 2022. 16(1): p. 297-314.
842 [35]. How, P., et al., Greenland-wide inventory of ice marginal lakes using a multi-method approach. Scientific
843 Reports, 2021. 11(1): p. 4481.
844 [36]. Ashraf, A., R. Naz and M.B. Iqbal, Altitudinal dynamics of glacial lakes under changing climate in the Hindu
845 Kush, Karakoram, and Himalaya ranges. Geomorphology, 2017. 283: p. 72-79.
846 [37]. Roy, D.P., et al., Landsat-8: Science and product vision for terrestrial global change research. Remote
847 Sensing of Environment, 2014. 145: p. 154-172.
848 [38]. Williamson, A.G., et al., Dual-satellite (Sentinel-2 and Landsat 8) remote sensing of supraglacial lakes in
849 Greenland. The Cryosphere, 2018. 12(9): p. 3045-3065.
850 [39]. Paul, F., et al., Glacier shrinkage in the Alps continues unabated as revealed by a new glacier inventory from
851 Sentinel-2. Earth System Science Data, 2020. 12(3): p. 1805-1821.
852 [40]. Zhang, M., F. Chen and B. Tian, An automated method for glacial lake mapping in High Mountain Asia
853 using Landsat 8 imagery. Journal of Mountain Science, 2018. 15(1): p. 13-24.
854 [41]. Sheng, Y., et al., Representative lake water extent mapping at continental scales using multi-temporal
855 Landsat-8 imagery. Remote Sensing of Environment, 2016. 185: p. 129-141.
856 [42]. Wang, J., Y. Sheng and Y. Wada, Little impact of the Three Gorges Dam on recent decadal lake decline
857 across China's Yangtze Plain. Water Resources Research, 2017. 53(5): p. 3854-3877.
858 [43]. Wang, J., et al., Recent global decline in endorheic basin water storages. Nature Geoscience, 2018. 11(12):
859 p. 926-932.
860 [44]. Wangchuk, S. and T. Bolch, Mapping of glacial lakes using Sentinel-1 and Sentinel-2 data and a random
861 forest classifier: Strengths and challenges. Science of Remote Sensing, 2020. 2: p. 100008.
862 [45]. Zhao, W., et al., Lake area monitoring based on land surface temperature in the Tibetan Plateau from 2000
863 to 2018. ENVIRONMENTAL RESEARCH LETTERS, 2020. 15(0840338).
864 [46]. Yao, X., et al., Definition and classification system of glacial lake for inventory and hazards study. Journal
865 of Geographical Sciences, 2018. 28(2): p. 193-205.
866 [47]. Carrivick, J.L. and D.J. Quincey, Progressive increase in number and volume of ice-marginal lakes on the
867 western margin of the Greenland Ice Sheet. Global and Planetary Change, 2014. 116: p. 156-163.
868 [48]. Carrivick, J.L. and F.S. Tweed, Proglacial lakes: character, behaviour and geological importance. Quaternary
869 Science Reviews, 2013. 78: p. 34-52.
870 [49]. Li, D., D. Shangguan and M.N. Anjum, Glacial Lake Inventory Derived from Landsat 8 OLI in 2016–2018
871 in China–Pakistan Economic Corridor. ISPRS international journal of geo-information, 2020. 9(5): p. 294.
872 [50]. Emmer, A. and V. Cuřín, Can a dam type of an alpine lake be derived from lake geometry? A negative result.
873 Journal of Mountain Science, 2021. 18(3): p. 614-621.
874 [51]. RGI Consortium, Randolph Glacier Inventory – A Dataset of Global Glacier Outlines: Version 6.0:
875 Technical Report. 2017: Global Land Ice Measurements from Space, Colorado, USA.

876   [52]. Rose, A., et al., LandScan Global 2020. 2021, Oak Ridge National Laboratory: Oak Ridge, TN.

877   [53]. Yao, C., et al., Temporal and Spatial Changes of Glacial Lakes in the China-Pakistan Economic Corridor
878   from 1990 to 2018. Journal of Glaciology and Geocryology, 2020. 42(01): p. 33-42.

879   [54]. Ullah, S., et al., Observed changes in maximum and minimum temperatures over China- Pakistan economic
880   corridor during 1980－2016. Atmospheric Research, 2019. 216: p. 37-51.

881   [55]. Kääb, A., et al., Contrasting patterns of early twenty-first-century glacier mass change in the Himalayas.
882   Nature, 2012. 488(7412): p. 495-498.

883   [56]. Yao, T., et al., Different glacier status with atmospheric circulations in Tibetan Plateau and surroundings.
884   NATURE CLIMATE CHANGE, 2012. 2(9): p. 663-667.

885   [57]. Hugonnet, R., et al., Accelerated global glacier mass loss in the early twenty-first century. Nature, 2021.
886   592(7856): p. 726-731.

887   [58]. Hewitt, K., The Karakoram Anomaly? Glacier Expansion and the 'Elevation Effect,' Karakoram
888   Himalaya. Mountain Research and Development, 2005. 25(4): p. 332-340.

889   [59]. Bolch, T., et al., Brief communication: Glaciers in the Hunza catchment (Karakoram) have been nearly in
890   balance since the 1970s. The Cryosphere, 2017. 11(1): p. 531-539.

891   [60]. Azam, M.F., et al., Glaciohydrology of the Himalaya-Karakoram. Science, 2021. 373(6557): p. eabf3668.

892   [61]. Wulder, M.A., et al., Current status of Landsat program, science, and applications. Remote Sensing of
893   Environment, 2019. 225: p. 127-147.

894   [62]. Nie, Y., et al., Glacial change in the vicinity of Mt. Qomolangma (Everest), central high Himalayas since
895   1976. Journal of Geographical Sciences, 2010. 20(5): p. 667-686.

896   [63]. Jiang, S., et al., Glacier Change, Supraglacial Debris Expansion and Glacial Lake Evolution in the Gyirong
897   River Basin, Central Himalayas, between 1988 and 2015. Remote Sensing, 2018. 10(7): p. 986.

898   [64]. Pfeffer, W.T., et al., The Randolph Glacier Inventory: a globally complete inventory of glaciers. Journal of
899   Glaciology, 2014. 60(221): p. 537-552.

900   [65]. Sakai, A., Brief communication: Updated GAMDAM glacier inventory over high-mountain Asia. The
901   Cryosphere, 2019. 13(7): p. 2043-2049.

902   [66]. Jarvis, A., et al., Hole-filled seamless SRTM data V4. 2008. 2008, International Centre for Tropical
903   Agriculture (CIAT): available from http://srtm.csi.cgiar.org.

904   [67]. Farr, T.G., et al., The Shuttle Radar Topography Mission. Reviews of Geophysics, 2007. 45(2): p. RG2004.

905   [68]. Rabus, B., et al., The shuttle radar topography mission—a new class of digital elevation models acquired by
906   spaceborne radar. ISPRS Journal of Photogrammetry and Remote Sensing, 2003. 57(4): p. 241-262.

907   [69]. Post, A. and L.R. Mayo, Glacier dammed lakes and outburst floods in Alaska: U.S. Geological Survey
908   Hydrologic Investigations Atlas 455. 1971, U.S. Geological Survey. p. 1-10.

909   [70]. Martín, C.N.S., et al., Proglacial landform assemblage in a rapidly retreating cirque glacier due to
910   temperature increase since 1970, Fuegian Andes, Argentina. Geomorphology, 2021. 390: p. 107861.

911   [71].Westoby, M.J., et al., Modelling outburst floods from moraine-dammed glacial lakes. Earth-Science Reviews,
912   2014. 134: p. 137-159.

913   [72]. Chen, X., et al., Dam-break risk analysis of the Attabad landslide dam in Pakistan and emergency
914   countermeasures. Landslides, 2017. 14(2): p. 675-683.

915   [73]. Wang, J., Y. Sheng and T.S.D. Tong, Monitoring decadal lake dynamics across the Yangtze Basin
916   downstream of Three Gorges Dam. Remote Sensing of Environment, 2014. 152(0): p. 251-269.

917   [74]. Nie, Y., et al., Reconstructing the Chongbaxia Tsho glacial lake outburst flood in the Eastern Himalaya:
918   Evolution, process and impacts. Geomorphology, 2020. 370(12): p. 107393.

919   [75]. McFeeters, S.K., The use of the Normalized Difference Water Index (NDWI) in the delineation of open

920   water features. International Journal of Remote Sensing, 1996. 17(7): p. 1425 - 1432.

921   [76]. Cook, S.J. and D.J. Quincey, Estimating the volume of Alpine glacial lakes. Earth Surf. Dynam., 2015. 3(4):
922   p. 559-575.

923   [77]. Hanshaw, M.N. and B. Bookhagen, Glacial areas, lake areas, and snow lines from 1975 to 2012: status of
924   the Cordillera Vilcanota, including the Quelccaya Ice Cap, northern central Andes, Peru. The Cryosphere, 2014.
925   8(2): p. 359-376.

926   [78]. Lyons, E.A., et al., Quantifying sources of error in multitemporal multisensor lake mapping. International
927   Journal of Remote Sensing, 2013. 34(22): p. 7887-7905.

928   [79]. Salerno, F., et al., Glacial lake distribution in the Mount Everest region: Uncertainty of measurement and
929   conditions of formation. GLOBAL AND PLANETARY CHANGE, 2012. 92-93: p. 30-39.

930   [80]. Miles, E.S., et al., Glacial and geomorphic effects of a supraglacial lake drainage and outburst event, Everest
931   region, Nepal Himalaya. The Cryosphere, 2018. 12(12): p. 3891-3905.

932   [81]. Liu, Q. and C. Mayer, Distribution and interannual variability of supraglacial lakes on debris-covered
933   glaciers in the Khan Tengri-Tumor Mountains, Central Asia. Environmental Research Letters, 2015. 10(1): p.
934   014014.

935   [82]. Wu, R., et al., A Deep Learning Method for Mapping Glacial Lakes from the Combined Use of Synthetic-
936   Aperture Radar and Optical Satellite Images. Remote Sensing, 2020. 12(24): p. 4020
937   .
938

第 26 页: [1] 带格式的	QIU	10/11/2022 9:02:00 PM

第 26 页: [2] 带格式的	QIU	9/29/2022 3:56:00 PM

: 9

第 26 页: [3] 带格式的	QIU	9/29/2022 3:55:00 PM

: 1.15

第 26 页: [4] 带格式的	QIU	9/29/2022 3:55:00 PM

, : 1.15

第 26 页: [5] 带格式的	QIU	9/29/2022 3:55:00 PM

: 1.15

第 26 页: [6] 带格式的	QIU	9/29/2022 3:55:00 PM

, : 1.15

第 26 页: [7] 带格式的	QIU	9/29/2022 3:56:00 PM

: 9

第 26 页: [8] 带格式的	QIU	9/29/2022 3:55:00 PM

: 1.15

第 26 页: [9] 带格式的	QIU	9/29/2022 3:55:00 PM

, : 1.15

第 26 页: [10] 带格式的	QIU	9/29/2022 3:55:00 PM

: 1.15

第 26 页: [11] 带格式的	QIU	9/29/2022 3:55:00 PM

, : 1.15

第 26 页: [12] 带格式的	QIU	9/29/2022 3:56:00 PM

: 9

第 26 页: [13] 带格式的	QIU	9/29/2022 3:55:00 PM

: 1.15

第 26 页: [14] 带格式的	QIU	9/29/2022 3:55:00 PM

, : 1.15

第 26 页: [15] 带格式的	QIU	9/29/2022 3:55:00 PM

: 1.15

第 26 页: [16] 带格式的	QIU	9/29/2022 3:56:00 PM

: 9

第 26 页: [17] 带格式的	QIU	9/29/2022 3:55:00 PM

: 1.15

第 26 页: [18] 带格式的	QIU	9/29/2022 3:55:00 PM
, : 1.15		
第 26 页: [19] 带格式的	QIU	9/29/2022 3:55:00 PM
: 1.15		
第 26 页: [20] 带格式的	QIU	9/29/2022 3:56:00 PM
: 9		
第 26 页: [21] 带格式的	QIU	9/29/2022 3:55:00 PM
: 1.15		
第 26 页: [22] 带格式的	QIU	9/29/2022 3:56:00 PM
: 9		
第 26 页: [22] 带格式的	QIU	9/29/2022 3:56:00 PM
: 9		
第 26 页: [23] 带格式的	QIU	9/29/2022 3:55:00 PM
, : 1.15		
第 26 页: [24] 带格式的	QIU	9/29/2022 3:55:00 PM
: 1.15		
第 26 页: [25] 带格式的	QIU	9/29/2022 3:56:00 PM
: 9		
第 26 页: [26] 带格式的	QIU	9/29/2022 3:55:00 PM
: 1.15		
第 26 页: [27] 带格式的	QIU	9/29/2022 3:55:00 PM
, : 1.15		
第 26 页: [28] 带格式的	QIU	9/29/2022 3:56:00 PM
: 9		
第 26 页: [28] 带格式的	QIU	9/29/2022 3:56:00 PM
: 9		
第 26 页: [29] 带格式的	QIU	9/29/2022 3:55:00 PM
: 1.15		
第 26 页: [30] 带格式的	QIU	9/29/2022 3:56:00 PM
: 9		
第 26 页: [31] 带格式的	QIU	9/29/2022 3:55:00 PM
: 1.15		
第 26 页: [32] 带格式的	QIU	9/29/2022 3:55:00 PM
, : 1.15		
第 26 页: [33] 带格式的	QIU	9/29/2022 3:55:00 PM
: 1.15		

第 26 页: [34] 带格式的	QIU	9/29/2022 3:56:00 PM
: 9		

第 26 页: [35] 带格式的	QIU	9/29/2022 3:55:00 PM
: 1.15		

第 26 页: [36] 带格式的	QIU	9/29/2022 3:55:00 PM
, : 1.15		

第 26 页: [37] 带格式的	QIU	9/29/2022 3:56:00 PM
: 9		

第 26 页: [38] 带格式的	QIU	9/29/2022 3:56:00 PM
: 9		

第 26 页: [39] 带格式的	QIU	9/29/2022 3:55:00 PM
: 1.15		

第 26 页: [40] 带格式的	QIU	9/29/2022 3:56:00 PM
: 9		

第 26 页: [41] 带格式的	QIU	9/29/2022 3:55:00 PM
: 1.15		

第 26 页: [42] 带格式的	QIU	9/29/2022 3:55:00 PM
, : 1.15		

第 26 页: [43] 带格式的	QIU	9/29/2022 3:55:00 PM
: 1.15		

第 26 页: [44] 带格式的	QIU	9/29/2022 3:56:00 PM
: 9		

第 26 页: [45] 带格式的	QIU	9/29/2022 3:55:00 PM
: 1.15		

第 26 页: [46] 带格式的	QIU	9/29/2022 3:55:00 PM
, : 1.15		

第 26 页: [47] 带格式的	QIU	9/29/2022 3:55:00 PM
: 1.15		

第 26 页: [48] 带格式的	QIU	9/29/2022 3:56:00 PM
: 9		

第 26 页: [49] 带格式的	QIU	9/29/2022 3:55:00 PM
: 1.15		

第 26 页: [50] 带格式的	QIU	9/29/2022 3:55:00 PM
, : 1.15		

第 26 页: [51] 带格式的	QIU	9/29/2022 3:55:00 PM
: 1.15		

第 26 页: [52] 带格式的	QIU	9/29/2022 3:35:00 PM
第 26 页: [53] 带格式的	QIU	9/29/2022 3:35:00 PM
：		
第 26 页: [54] 带格式的	AppleYN	9/15/2022 8:55:00 AM
：		
第 26 页: [55] 带格式的	AppleYN	9/15/2022 8:55:00 AM